

Angular Momentum and Vortex Formation in Bose-Einstein-Condensed Cold Dark Matter Haloes

Tanja Rindler-Daller^{1,2*} and Paul R. Shapiro^{1†}

¹ *Department of Astronomy and Texas Cosmology Center, The University of Texas at Austin, Austin, TX 78712, USA*

² *Institut für Theoretische Physik, Universität zu Köln, 50937 Cologne, Germany*

December 23, 2011

ABSTRACT

Various extensions of the standard model of particle physics predict the existence of very light bosons, with masses ranging from about 10^{-5} eV for the QCD axion down to 10^{-33} eV for ultra-light particles. These particles could be responsible for all or part of the cold dark matter (CDM) in the Universe. For such particles to serve as CDM, their phase-space density must be high enough to form a Bose-Einstein condensate (BEC). The fluid-like nature of BEC-CDM dynamics differs from that of standard collisionless CDM, however, so different signature effects on galactic haloes may allow observations to distinguish them. Standard CDM has problems with galaxy observations on small scales; cuspy central density profiles of haloes and the overabundance of subhaloes seem to conflict with observations of dwarf galaxies. It has been suggested that BEC-CDM can overcome these shortcomings for a large range of particle mass m and self-interaction coupling strength g . For quantum-coherence to influence structure on the scale of galactic haloes of radius R and mass M , either the de-Broglie wavelength $\lambda_{dB} \lesssim R$, which requires $m \gtrsim m_H \cong 10^{-25}(R/100 \text{ kpc})^{-1/2}(M/10^{12} \text{ M}_\odot)^{-1/2}$ eV, or else $\lambda_{dB} \ll R$ but gravity is balanced by self-interaction, which requires $m \gg m_H$ and $g \gg g_H \cong 2 \cdot 10^{-64}(R/100 \text{ kpc})(M/10^{12} \text{ M}_\odot)^{-1}$ eV cm³. Here we study the largely-neglected effects of angular momentum on BEC haloes. Dimensionless spin parameters $\lambda \simeq 0.05$ are expected from tidal-torquing by large-scale structure formation, just as for standard CDM. Since laboratory BECs develop quantum vortices if rotated rapidly enough, we ask whether this amount of angular momentum is sufficient to form vortices in BEC haloes, which would affect their structure with potentially observable consequences. The minimum angular momentum required for a halo to sustain a vortex, L_{QM} , corresponds to \hbar per particle, or $\hbar M/m$. For $\lambda = 0.05$, this requires $m \geq 9.5m_H$, close enough to the particle mass required to influence structure on galactic scales that BEC haloes may be subject to vortex formation. While this is a necessary condition, it is not sufficient. To determine if and when quantum vortices will form in BEC halos with a given λ -value, we study the equilibrium of self-gravitating, rotating, virialized BEC haloes which satisfy the Gross-Pitaevskii-Poisson equations, and calculate under what conditions vortices are energetically favoured, in two limits: either just enough angular momentum for one vortex or a significant excess of angular momentum. For $\lambda = 0.05$, vortex formation is energetically favoured for $L/L_{QM} \geq 1$ as long as *both* $m/m_H \geq 9.5$ and $g/g_H \geq 68.0$. Hence, vortices are expected for a wide range of BEC parameters. However, vortices cannot form for vanishing self-interaction (i.e. when $\lambda_{dB} \lesssim R$), and a range of particle parameters also remains even for BEC haloes supported by self-interaction, for which vortices will *not* form. Such BEC haloes can be modelled by compressible, $(n = 1)$ -polytropic, irrotational Riemann-S ellipsoids.

Key words: cosmology: theory - dark matter - galaxies: haloes - galaxies: kinematics and dynamics - methods: analytical

* daller@astro.as.utexas.edu

† shapiro@astro.as.utexas.edu

1 INTRODUCTION

In the last decades, astronomical observations have provided a range of supporting evidence that about 23 % of the energy density of the Universe is comprised of non-baryonic dark matter. Its particle nature is still unknown, but all candidates find their justification in extensions of the standard model of particle physics. Based on observations, it is now believed that dark matter is weakly-interacting and non-relativistic, hence behaving like a cold gas, and generally termed cold dark matter (CDM).

The standard form of CDM is often supposed to be a relic of the Big Bang in the form of weakly-interacting, massive particles (WIMPs), in particular, the lightest supersymmetric particles, the most popular of which is the neutralino, with particle mass of the order of 100 GeV. Efforts are underway to measure the presence of those particles, but no direct detection has yet been reported. On the other hand, as far as the dynamics of galaxies and large-scale structure is concerned, standard CDM is modelled as a cold, collisionless gas with vanishing pressure. While many observational properties of galaxies can be reproduced, some crucial issues are subject to controversy. Simulations of standard CDM structure formation predict a universal halo density profile, which has a cusp going like r^{-1} in the center. This seems to be in conflict with the observational properties of low-surface brightness (LSB) and dwarf galaxies. Moreover, standard CDM predicts the hierarchical merger of smaller structures into larger structures over time, with an overly abundant population of subhaloes inside a halo like the Local Group for which there does not seem to be an observational counterpart. Given the above shortcomings, and the null results of direct detection experiments to date, we are still free to consider other candidates for the CDM paradigm.

Another major candidate for dark matter is the QCD axion, the pseudo-Nambu-Goldstone boson of the Peccei-Quinn phase transition, proposed as a dynamical solution to the CP-problem of the strong interactions. For the axion to be CDM, it has to be very light, $m \sim 10^{-5}$ eV, and direct detection experiments rely on its electro-dynamical coupling, employing the haloscope idea of Sikivie (1983) in the ADMX experiment (Asztalos et al. (2010)), and axion-photon oscillations in the presence of high magnetic fields using lasers (so-called light-shining-through-wall experiments), e.g. Chou et al. (2008).

In addition to the QCD axion, multidimensional cosmological and string theories generically predict the existence of even much lighter bosonic particles down to masses of the order of 10^{-33} eV (see e.g. Horava & Witten (1996); Günther & Zhuk (1997)), which could form all or part of the dark matter¹, e.g. Carroll (1998); Arkani-Hamed, Dimopoulos & Dvali (1999); Arvanitaki et al. (2010). For such particles to serve as CDM, their phase-space density must be high enough to form a Bose-Einstein condensate (BEC), i.e. a macroscopic occupancy of the many-body ground state. Generally,

for a system to undergo Bose-Einstein condensation, the phase-space density $n\lambda_{deB}^3$ must exceed a number of order one, where n is the number density and λ_{deB} is the de-Broglie wavelength of the particles. While for axions $n\lambda_{deB}^3 \gg 1$, ultra-light bosons even fulfill $n\lambda_{deB}^3 \gg 1$. It has been shown in models by Silverman & Mallet (2002), Ureña-López (2009) and Lundgren et al. (2010) that ultra-light particles are able to undergo a phase transition in the early universe to a BEC at a temperature which is well above that of the time of recombination. These bosons are thereby able to form a non-relativistic, quantum-degenerate gas, in contrast to the (fermionic) neutrinos which remain relativistic. While numerous searches for the QCD axion are currently pursued, the ultra-light bosons seem to be out of reach for direct detection. However, low-temperature ultra-precision experiments promise new possibilities to search directly even for these ultra-light particles, for a review see e.g. Jäckel & Ringwald (2010). An interesting, but very challenging experimental proposal for detecting such particles, by exploiting their supposed coupling to gluons, has been presented recently by Graham & Rajendran (2011). Nevertheless, this kind of dark matter will best be traced in the near future through the signature of its dynamical differences from standard CDM, an aspect of which we will study in this paper. A full account of all the existing literature is beyond the scope of this paper, but earlier investigations of models for light bosonic dark matter include e.g. the works of Ipser & Sikivie (1983); Baldeschi, Gelmini & Ruffini (1983); Khlopov, Malomed & Zeldovich (1985); Membrado, Pacheco & Sañude (1989); Press, Ryden & Spergel (1990); Widrow & Kaiser (1993); Sin (1994); Schunck (1998); Lee & Koh (1996); Schunck, Fuchs & Mielke (2006) and Matos & Ureña-López (2001) to name a few. Most of this literature has been restricted to free particles without self-interaction.

We will see that BEC cold dark matter (henceforth also BEC-CDM) obeys quantum-mechanical *fluid equations*. Therefore, small-scale structure can be very different for BEC dark matter from that of collisionless standard CDM. The behaviour of *self-interacting*² BEC-CDM as a superfluid makes possible entirely new phenomena like the formation of *quantum vortices*. Astronomical observations may thus provide a means to diagnose different dynamical effects, thereby allowing us to constrain (or rule out) this form of dark matter. In fact, BEC-CDM has previously been invoked to overcome the above mentioned shortcomings of standard CDM: One prime motivation for considering BECs for CDM has been their ability to produce galactic haloes with constant density cores, see e.g. Goodman (2000) ("repulsive DM") and Peebles (2000) ("fluid DM"), since the corresponding profiles may then better agree with observed rotation curves of dwarf and LSB galaxies as has been

¹ While those particles all the way up to the QCD axion are often summarized as 'axion-like' particles, we will avoid this term here, since the definition of what is 'axion-like' may sometimes encompass particles in the keV mass range. Instead, we will refer to them as ultra-light bosons.

² This is different from the kind of self-interacting, cold dark matter particles referred to elsewhere in the literature as SIDM, suggested by Spergel & Steinhardt (2000), which we have studied in Ahn & Shapiro (2005) and Koda & Shapiro (2011). In SIDM, the particle self-interaction results in 2-body elastic scattering which adds 'collisionality' to the otherwise collisionless CDM gas, but does not make a BEC or exhibit any form of macroscopic quantum coherence. The reader should henceforth avoid any confusion between the BEC-CDM discussed here and SIDM.

shown in the papers of Arbey, Lesgourges & Salati (2003); Böhmer & Harko (2007) and Böhmer, Martins, Salucci (private communication). The problem of overabundance of sub-haloes in standard CDM is naturally resolved in some BEC dark matter models, since the uncertainty principle prevents the formation of gravitationally bound isolated structures below a certain length scale, which depends on the dark matter particle mass, see e.g. Hu, Barkana & Gruzinov (2000) ("fuzzy DM"). However, the formation of large-scale structures involving BEC dark matter has not yet been studied in the same depth as for standard CDM and many issues are still unresolved. Some recent results on structure formation studies involving BEC-CDM can be found in the works of Ureña-López & Guzmán (2003); Fukuyama, Morikawa & Tatekawa (2008); Woo & Chiueh (2009); Marsh & Ferreira (2010); Harko (2011) and Chavanis (2012)³.

We will see in the next section that for quantum-coherence to influence structure on the scale of galactic haloes of radius R , either the de-Broglie wavelength of the dark matter particle is of that same order,

$$\lambda_{dB} \lesssim R,$$

requiring the particle mass to be of the order

$$m \gtrsim m_H \cong 10^{-25} (R/100 \text{ kpc})^{-1/2} (M/10^{12} M_\odot)^{-1/2} \text{ eV},$$

or else

$$\lambda_{dB} \ll R$$

and the halo is supported against gravity by self-interaction pressure, which requires *both*

$$m \gg m_H$$

and

$$g \gg g_H \cong 2 \cdot 10^{-64} (R/100 \text{ kpc}) (M/10^{12} M_\odot)^{-1} \text{ eV cm}^3,$$

and we choose units where $c = 1$.

However, previous literature on BEC-CDM has mostly neglected an important aspect of halo physics, namely angular momentum. In the early phases of halo collapse, tidal torques caused by large-scale structure give a halo most of its angular momentum. Cosmological N-body simulations of the standard CDM universe show that haloes form with a net angular momentum such that the dimensionless ratio

$$\lambda = \frac{L|E|^{1/2}}{GM^{5/2}}, \quad (1)$$

which expresses their degree of rotational support, has typical values in the range $[0.01, 0.1]$ with median value $\simeq 0.05$. These values can be found in Barnes & Efstathiou (1987), and more recently in Antonucci et al. (2010), which seem to be confirmed by observations, see Hernandez et al. (2007).

³ Slepian & Goodman (2011) recently suggested that astronomical constraints can be used to rule out strongly-repulsive bosonic dark matter. However, their analysis does not apply to the case considered here. They assume that the bosons are in thermodynamic equilibrium in isothermal haloes at the halo virial temperature, with a condensate core surrounded by a non-condensate envelope. As they themselves point out, their assumption breaks down when 2-body collisions are not frequent enough, which is the case here (see also Section 5).

In the above expression, L is the total angular momentum, E is the total energy, and M is the total mass of the halo. The quantity λ^2 corresponds roughly to the so-called t -parameter, $t \equiv T/|W|$, where T is the rotational kinetic energy and W is the gravitational potential energy. Tidal-torque theory can successfully account for the λ -values found in N -body simulations of structure formation, see e.g. Porciani, Dekel & Hoffman (2002a,b). We shall here be interested in the case where the BEC nature of CDM affects small-scale structure and the internal dynamics of galactic haloes, while large-scale structure formation follows that of standard CDM to a great extent. In this paper, therefore we will adopt the above range of λ -values for BEC-CDM haloes, too. The general problem of *acquisition* of angular momentum by BEC haloes is worth further consideration in a future work, but in the context of this work, we will content ourselves with the convenience of the above prescription.

Once haloes rotate, additional effects come into play. Halo shapes and profiles will differ from those which result when angular momentum is zero, and, since self-interacting BEC-CDM behaves as an irrotational superfluid, these will differ from the case of collisionless CDM. In addition, it is known that laboratory BECs can develop quantum vortices when rotated with a sufficient angular velocity (see e.g. Madison et al. (2000)), thereby changing the density profile in a characteristic way. The question arises as to whether this may be also possible for BEC haloes and we will attempt to answer that question here.

Several authors have previously pursued related questions. Silverman & Mallet (2002) postulated vortices in galactic haloes comprised of ultra-light bosonic particles by comparing the critical angular velocity for vortex formation with the rotation rate of M31. However, the formula quoted there without derivation applies actually to laboratory superfluids with strong self-interaction but without self-gravity. Subsequently, Yu & Morgan (2002) have studied the influence of a vortex lattice on the velocity profile of a spherical galactic halo composed of ultra-light bosons.

On the other hand, Duffy & Sikivie (2008) have argued that certain fine-structure in the observed inner mass distribution of the Milky Way can be explained only if the infalling dark matter particles had a net overall rotation, causing a 'tricuspid' caustic ring in the catastrophe structure of dark matter in that case. For standard, non-interacting CDM models, however, one expects infall to be *irrotational*. According to Sikivie & Yang (2009), axionic dark matter, as a BEC, may be able to form a vortex lattice with high enough vorticity so as to mimic a net rotational component, producing the above structure. As such, the authors suggest, Milky-Way observations may already have detected the signature of axionic dark matter. We will come back to this claim in Section 5.

This paper will extend the analysis which we presented in Rindler-Daller & Shapiro (2010). We showed there that vortices are favoured to form for a wide range of possible particle mass and self-interaction strength, by calculating for the first time the critical angular velocity for vortex creation for a simple model of BEC-CDM galactic haloes and comparing the result with the angular velocity expected from cosmological N-body simulations of standard CDM haloes. Kain & Ling (2010) subsequently studied the formation of a vortex in spherical (non-rotating) haloes in the Thomas-

Fermi regime of strong self-interaction. The major drawback of their approach is the fact that it starts from haloes which have no angular momentum. The physical mechanism by which vortices shall form is thus absent from the beginning. In fact, the amount of angular momentum of a singly-quantized, axisymmetric vortex in the center of a halo is given by

$$L_{QM} \equiv N\hbar, \quad (2)$$

and this angular momentum has to be provided by halo spinning. We will report here our study of the equilibrium of rotating, self-gravitating, virialized haloes, and the conditions for which vortex formation is favoured. For the latter, we will focus our attention on two extreme cases, one in which haloes have just enough angular momentum to support a single vortex, i.e. their angular momentum is $L = L_{QM}$, and the other case in which haloes have much excess angular momentum, such that $L \gg L_{QM}$. Haloes will be modelled in each case as rotating, ellipsoidal bodies. While the main conclusion of Rindler-Daller & Shapiro (2010) will not change, this paper will significantly improve on the analytic modeling of BEC haloes presented there and thereby establish better constraints on the BEC dark matter particle mass and self-interaction required for vortex formation to happen. We will employ an energy analysis of the full equations of motion, thereby deriving analytically the conditions under which vortex formation lowers the energy and is, hence, favoured in haloes with the amount of angular momentum expected from large-scale structure in the CDM universe.

The impact of vortices may be profound: We can expect vortices to reside preferentially in the centers of dark matter haloes. Vortices deplete the dark matter density in their core region once they have formed. This in turn influences the dark matter density profile and also the gravitational coupling to the baryons. If less dark matter is around than without vortices, for example, then baryon cooling and condensation, a prerequisite for star formation, may as a consequence be reduced and delayed. It is thus interesting to ask for which BEC-CDM models such vortices can be expected to form. However, we stress that this work will be a 'dark matter only'-analysis, and the baryonic component of galactic haloes will not be considered.

This paper is organized as follows: In *Section 2*, we review the basic equations, the self-interaction regimes of BEC dark matter and their consequences for halo density profiles. The underlying equations we are going to use are the Gross-Pitaevskii equation for the wave function of the Bose-Einstein-condensed halo, and the Poisson equation by which the density is coupled to the halo gravitational potential. The equation of motion can be restated in terms of quantum-mechanical fluid equations. So, in *Section 3* we will study approximate figures of equilibrium models for BEC haloes with angular momentum included: rotating haloes will be approximated either by irrotational Riemann-S ellipsoids or by Maclaurin spheroids. In *Section 4*, we will present the energy analysis to determine when vortex formation will occur in such BEC haloes, whose net amount of angular momentum we will fix by values for the λ -spin parameter, which are representative of those of standard CDM. In the regime of strong self-interaction, we will thereby establish bounds on the BEC dark matter particle mass and self-interaction strength above which vortices will be favoured. The implica-

tions of our results for halo models comprised of BEC-CDM will be presented in *Section 5*, which contains our conclusions and discussion. Some further detailed derivations, tables and frequently used relationships are deferred to three appendices.

2 FUNDAMENTALS OF BEC DARK MATTER HALOES

2.1 Basic equations

We will describe self-gravitating BEC haloes by self-consistently coupling the Gross-Pitaevskii (GP) equation of motion for the complex scalar BEC wavefunction $\psi(\mathbf{r}, t)$ (see e.g. Pitaevskii & Stringari (2003)) of the dark matter halo to the Poisson equation,

$$i\hbar \frac{\partial \psi}{\partial t} = -\frac{\hbar^2}{2m} \Delta \psi + (m\Phi + g|\psi|^2)\psi, \quad (3)$$

$$\Delta \Phi = 4\pi G m |\psi|^2, \quad (4)$$

where $|\psi|^2(\mathbf{r}, t) = n(\mathbf{r}, t)$ is the number density of dark matter particles of mass m and $\Phi(\mathbf{r})$ is the gravitational potential of the halo. We assume that *all* N particles comprising a given halo of volume V are in the condensed state described by ψ , such that

$$\int_V |\psi|^2 = N. \quad (5)$$

This effectively amounts to assuming that the gas is at zero temperature. Self-gravitating BEC matter has been considered before as a possible candidate for making ultradense stars, called boson stars, that can avoid collapse to a black hole (see e.g. Kaup (1968); Ruffini & Bonazzola (1969); Colpi, Shapiro & Wasserman (1986)). BEC haloes can be imagined as boson stars on galactic scales, except that their densities are very low. General-relativistic effects are thus usually considered to be negligible on those scales. As such, we are free here to treat the effects of gravity in the Newtonian limit, as is customary in the literature on BEC haloes.

BEC-CDM, like standard CDM, is assumed to interact so weakly with other matter and radiation, once its abundance is fixed in the early universe, that we can neglect all other, non-gravitational couplings. However, in contrast to standard CDM, BEC dark matter can be *self-interacting*. The BEC self-interaction has been included in equ.(3) in the usual way in terms of an effective interaction potential $g|\psi|^4/2$ with coupling constant (or self-interaction strength) g . The possibly complicated particle interactions are simplified this way in the GP framework in the low-energy limit of a dilute gas: disregarding higher than 2-body interactions, the cross section for elastic scattering of indistinguishable particles becomes constant in the low-energy limit,

$$\sigma_s = 8\pi a_s^2, \quad (6)$$

with the s-wave scattering length a_s . The coupling constant of the effective interaction is then given by

$$g = 4\pi\hbar^2 \frac{a_s}{m}. \quad (7)$$

In this work, we will restrict our consideration to $g \geq 0$ ($a_s \geq 0$). Condensates having attractive particle interactions

$g < 0$ have been shown not to support vortices, but rather produce bright solitons with which we will not be concerned here. We shall note that the above GP equation is strictly valid for dilute quantum gases only, which means that a_s must be much smaller than the mean interparticle distance, i.e. $a_s \ll n^{-1/3}$.

The complex wave function of the condensate in the GP equation, a form of non-linear Schrödinger equation (3), can be decomposed into its amplitude and phase function,

$$\psi(\mathbf{r}, t) = |\psi|(\mathbf{r}, t) e^{iS(\mathbf{r}, t)} = \sqrt{\frac{\rho(\mathbf{r}, t)}{m}} e^{iS(\mathbf{r}, t)} \quad (8)$$

with the corresponding dark matter halo mass density

$$\rho(\mathbf{r}, t) = m|\psi|^2. \quad (9)$$

Inserting (8) into (3), the GP equation decouples into two equations for the real functions $|\psi|$ and S ,

$$-\frac{2m}{\hbar} |\psi| \frac{\partial S}{\partial t} + \Delta |\psi| - |\psi| (\nabla S)^2 - \frac{2m}{\hbar^2} (m\Phi + g|\psi|^2) |\psi| = 0 \quad (10)$$

and

$$\frac{\partial |\psi|^2}{\partial t} + \nabla \cdot \left[|\psi|^2 \frac{\hbar}{m} \nabla S \right] = 0. \quad (11)$$

The associated quantum-mechanical current density,

$$\mathbf{j}(\mathbf{r}, t) = \frac{\hbar}{2im} (\psi^* \nabla \psi - \psi \nabla \psi^*) = n(\mathbf{r}, t) \frac{\hbar}{m} \nabla S(\mathbf{r}, t), \quad (12)$$

can be expressed in terms of the bulk velocity \mathbf{v} of the gas, if we write

$$\mathbf{v} = \frac{\hbar}{m} \nabla S. \quad (13)$$

The GP equation (3) can hence via equ.(10) and (11) be written as a system of quantum-mechanical hydrodynamic equations for the mass density ρ and the velocity \mathbf{v} , easily recast in the form of an Euler-like equation of motion along with the continuity equation,

$$\rho \frac{\partial \mathbf{v}}{\partial t} + \rho (\mathbf{v} \cdot \nabla) \mathbf{v} = -\rho \nabla Q - \rho \nabla \Phi - \nabla P_{SI}, \quad (14)$$

$$\frac{\partial \rho}{\partial t} + \nabla \cdot (\rho \mathbf{v}) = 0, \quad (15)$$

where we define

$$Q = -\frac{\hbar^2}{2m^2} \frac{\Delta \sqrt{\rho}}{\sqrt{\rho}}. \quad (16)$$

The term Q gives rise to what is often called 'quantum pressure', an additional force on the rhs of equ.(14) which basically stems from the quantum-mechanical uncertainty principle. The particle self-interaction, on the other hand, gives rise to a pressure of polytropic form

$$P_{SI} = K_p \rho^{1+1/n} \equiv \frac{g}{2m^2} \rho^2, \quad (17)$$

where the polytropic index is $n = 1$ (not to be confused with the number density $n(\mathbf{r}, t)$), and where the polytropic constant K_p depends only on the dark matter particle parameters. According to equations (14)-(17), BEC haloes as quantum gases have fluid-like properties, in contrast to the collisionless nature of standard CDM haloes.

The definition of the bulk velocity in equ.(13) implies that for any smooth phase function S , the velocity flow of the

system is *irrotational*, $\nabla \times \mathbf{v} = 0$, which is a typical characteristic of superfluids. However, in the presence of a vortex, the fluid velocity experiences a singularity and the circulation around a contour enclosing the vortex is non-vanishing and a multiple integer of the elementary circulation,

$$\oint_{\mathcal{C}} \nabla S \cdot d\mathbf{l} = 2\pi d \frac{\hbar}{m} \quad (18)$$

where $d\mathbf{l}$ is a unit tangent vector to the curve \mathcal{C} encircling the vortex with winding number d . The parameter d is an integer in order to ensure that the wave function, whose amplitude vanishes along the vortex, is singly-valued. The genuine quantum character of the system can be inferred by the fact that the above fluid circulation condition has effectively become a 'quantization condition'. For an axial-symmetric vortex, $S = d\phi$, the velocity flow around it is

$$\mathbf{v} = \frac{\hbar}{m} \frac{d}{r} \hat{\phi}. \quad (19)$$

A wavefunction having such a vortex is an eigenstate of the angular momentum with $l_z = d\hbar$, such that the vortex carries a total angular momentum equal to

$$L_z = dN\hbar \equiv dL_{QM}. \quad (20)$$

L_{QM} , as already defined in (2), is the minimum angular momentum necessary to sustain a singly-quantized vortex and will constitute an important quantity of the analysis in Section 3 and 4.

The hydrodynamic equations described above make it possible for us to apply familiar results for self-gravitating, classical fluids to derive properties of quantum-mechanical BEC dark matter (e.g. the classical figures of gravitational equilibrium, the properties of vorticity-free flow, the conditions leading to gravitational instability or vortex formation). In this way, we can also make clear the distinct role played by the quantum pressure term in the Euler equation in contrast to the roles of the polytropic self-interaction pressure and gravity. In the future, this will also be useful when we consider the dynamical origin of the virialized structures which constitute the cosmological haloes in this model, including the application of numerical hydrodynamic methods.

In this paper, however, we shall limit our treatment to the equilibrium structure of the virialized haloes expected to emerge during the cosmological formation of galaxies and large-scale structure in a BEC-CDM-dominated universe. The dynamical formation of such structures is presumed to result from the gravitational instability of primordial density fluctuations, like those in the standard CDM model, leading to the 'cosmic web' of filamentary structure. In order to follow the development of vortices, predicted here by a stability analysis, an initial-value problem involving the fully time-dependent 3D evolution from linear perturbations to the turn-around and nonlinear collapse of individual haloes must be solved, including the tidal torques responsible for halo angular momentum. This is a challenging task and beyond the scope of this paper. Here, instead, we take the first step of determining whether the virialized haloes in a BEC-CDM universe are subject to vortex formation by applying an energy argument to the stationary description of BEC-CDM haloes as rotating, self-gravitating figures of equilibrium. If the energy of such a halo is lower in the presence of a single, central vortex than without a vortex for some

values of the dark matter particle mass and self-interaction coupling strength, for rotation rates consistent with the angular momentum expected from large-scale structure formation, then the halo is unstable to vortex formation for those parameters. Before we turn our attention to rotating haloes, we set the stage by reviewing two important limiting cases which give insight into how the properties of the DM particle can lead to quantum-coherence on galactic scales.

2.2 BEC dark matter halo regimes

In this paper, we will study bound, isolated systems whose equilibrium structure must satisfy the Virial theorem (see relationship (59) in the next subsection)⁴. BEC haloes can be stabilized against gravitational collapse by internal pressure or rotation. In addition, BEC haloes can be prevented from collapse by the quantum-mechanical uncertainty principle, which is expressed by the quantum-kinetic term in (3). In order to gain an idea for the length scales involved, we may simply check the importance of terms of the time-independent GP equation in different limiting cases⁵. Obviously, the corresponding characteristic length scales will be determined by the respective particle or halo parameters which are involved in the terms under consideration. In the following, let R denote the size, M the total mass and $\bar{\rho}$ the mean density of a given halo.

2.2.1 Non-interacting DM particles: quantum pressure versus gravity

For quantum-coherence to be relevant on the scale of a halo, the dark matter particle de-Broglie wavelength

$$\lambda_{deB} = \frac{h}{mv}, \quad (21)$$

should be of the order of the size of the system

$$\lambda_{deB} \lesssim R. \quad (22)$$

Using $v_{vir} \simeq v_{circ} = (GM/R)^{1/2}$ in the expression for λ_{deB} , the particle mass must be of the order of

$$m \simeq \frac{h}{(GM R)^{1/2}} \simeq \frac{h}{R^2 (G\bar{\rho})^{1/2}}. \quad (23)$$

For galactic virial velocities of the order of $v_{vir} \sim 10 - 200$ km/s, it is clear that it is the particle mass which must be small enough in order for the de-Broglie wavelength to be comparable to the extent of the halo.

The quantum-kinetic term can stabilize a system against gravitational collapse,

$$0 = -\frac{\hbar^2}{2m} \Delta\psi + m\Phi\psi \quad (24)$$

above a length scale of

$$l_{QP} = \sqrt{\frac{\hbar}{m(2G\bar{\rho})^{1/2}}}, \quad (25)$$

which plays the role of a quantum Jeans length (see also Khlopov, Malomed & Zeldovich (1985); Hu, Barkana & Gruzinov (2000)). In BEC-CDM without self-interaction, l_{QP} is the smallest scale above which bound structures can form. More precisely, it can be shown that the density profile of a bound system like a halo, can only be determined numerically, and is given for instance in Membrado, Pacheco & Sañude (1989). It has a flat core and falls off as r^{-4} at infinity. Although the total mass $M = Nm$ is conserved and hence finite, the system has no finite size (i.e. no compact support) in this regime, and so one may calculate a radius which includes 99 % of the mass,

$$R_{99} = 9.9 \frac{\hbar^2}{GMm^2}, \quad (26)$$

Membrado, Pacheco & Sañude (1989). Indeed, this radius which is about 5 times as large as (25), is just the more accurate form of l_{QP} , which can be seen by expressing the density in (25) by using the total mass and radius, instead. Now, if we require λ_{deB} to be of the order of

$$l_{QP} \lesssim \lambda_{deB} \lesssim R, \quad (27)$$

the particle mass has to satisfy $m \lesssim \sqrt{18\pi^3} m_H$, where we have defined

$$m_H \equiv \frac{\hbar}{R^2 (\pi G \bar{\rho})^{1/2}} = \frac{2\hbar}{\sqrt{3G}} (RM)^{-1/2}, \quad (28)$$

depending on halo properties. This mass of a *non-interacting* DM particle is hence characteristic for making the dark matter of a halo quantum-coherent on a substantial fraction of its size.

There is, however, yet another meaning for this definition, which is of importance in the context of our paper: If a halo of mass M and angular momentum $L = L_{QM} \equiv N\hbar$ rotates uniformly with an angular velocity Ω_{QM} , then

$$L_{QM} = MR^2 \Omega_{QM} \quad (29)$$

implies

$$\Omega_{QM} = \frac{\hbar}{mR^2}. \quad (30)$$

On the other hand, the characteristic gravitational angular frequency is usually defined as

$$\Omega_G \equiv \sqrt{\pi G \bar{\rho}}. \quad (31)$$

It is basically the inverse free-fall time of a self-gravitating body, i.e. this angular velocity corresponds to a rotation, which supports the halo against gravitational collapse. Now, the dark matter particle mass assumes the form (28) if $\Omega_G = \Omega_{QM}$, i.e. if the halo's angular velocity due to gravitational stability is sufficient to have each particle contribute an amount of \hbar to the total angular momentum.

This regime, where self-interaction is neglected, is denoted as *Regime I* in Table 1.

⁴ The dynamical evolution which leads to the formation of the virialized haloes in a BEC-CDM cosmology is beyond the scope of this paper, which focuses on the haloes themselves. For some discussion of this dynamical evolution, the reader is referred to Alcubierre et al. (2002); Guzmán & Ureña-López (2004) and Short & Coles (2006).

⁵ A Jeans instability analysis in these limiting cases has been recently presented in Chavanis (2011).

2.2.2 Strongly-interacting DM particles: self-interaction pressure versus gravity

In the regime where the particle self-interaction dominates, the so-called *Thomas-Fermi (TF) regime*⁶, it is only the self-interaction which balances gravity,

$$0 = m\Phi\psi + g|\psi|^2\psi. \quad (32)$$

A system is then gravitationally bound above a length scale of

$$l_{SI} = \frac{1}{m} \sqrt{\frac{g}{G}}. \quad (33)$$

More precisely, the GP equation of state is *exactly* an $(n = 1)$ -polytropic law in this case, and equ.(14) reduces to a Lane-Emden equation of motion. Solving (51) with (52), or equivalently (14) in this regime, leads to the following general result for the mass density profile,

$$\rho(\mathbf{r}) = \frac{m}{g} \left(\mu - m\Phi - \frac{m}{2} \mathbf{v}^2 \right), \quad (34)$$

which can be determined, once Φ and \mathbf{v} are known. For spherical haloes in the static case, the density profile is given by

$$\rho^S(\mathbf{r}) = \rho_c^S \sin \left(\sqrt{\frac{2\pi G}{K_p}} r \right) / \left(\sqrt{\frac{2\pi G}{K_p}} r \right), \quad (35)$$

with the corresponding ratio of central to mean density as

$$\rho_c^S / \bar{\rho}^S = \pi^2 / 3 \simeq 3.29. \quad (36)$$

A spherical BEC halo is thus an $(n = 1)$ -polytrope with radius

$$R_0 = \pi \sqrt{\frac{K_p}{2\pi G}} = \pi \sqrt{\frac{g}{4\pi G m^2}}. \quad (37)$$

This result, derived in Chandrasekhar (1939) for stellar bodies, has been re-derived in the context of long-range-interacting atomic BEC gases in O'Dell et al. (2000) and in the context of dark matter, for instance in the works of Goodman (2000), Peebles (2000) and Böhmer & Harko (2007). The Thomas-Fermi regime will be studied in more detail in *Section 3*. Since this limit corresponds to the BEC becoming an $(n = 1)$ -polytrope, we will refer to this case also as the *polytropic regime*. The convenient simplifications, which come by disregarding the complicated quantum pressure term in (14) in this regime, have been heavily exploited in much of the literature on the subject. However, this comes with a price. According to equ.(37), the size of the polytrope is fixed by the BEC-CDM particle mass and coupling strength in the combination g/m^2 . While we shall continue to refer to this size as the halo size, it shall be understood that this refers *either* to the actual halo size *or* to the size of a virialized core region within a larger halo. The TF regime considered here is denoted as *Regime II* in Table 1.

⁶ The Thomas-Fermi energy functional appeared originally in atomic physics as an energy depending only on the density of the system. Since the GP energy, too, depends on density only in the above limit case, its formal analogy has been given the same name.

2.2.3 Validity of the Thomas-Fermi regime: quantum pressure versus self-interaction

To determine whether a halo is in *Regime I* or *II*, we must compare the quantum pressure and self-interaction pressure terms to each other. When the length scale for density variation in the BEC fluid is such that the two terms are of equal magnitude, that length scale is sometimes called the 'healing length'. The reason for this name is because it is the characteristic distance over which the wavefunction approaches the background value of a smooth density distribution, subjected to a localized perturbation. Balancing quantum-kinetic term and self-interaction,

$$0 = -\frac{\hbar^2}{2m} \Delta\psi + g|\psi|^2\psi, \quad (38)$$

results thus in the following expression for the healing length,

$$\xi = \frac{\hbar}{\sqrt{2\bar{\rho}g}}. \quad (39)$$

We will see below that if the system's characteristic size is much larger than this, $R \gg \xi$, than⁷ the quantum pressure can be neglected compared to the self-interaction term and we are in the Thomas-Fermi regime (*Regime II*). For a given mean halo density $\bar{\rho}$, we see that ξ grows with decreasing coupling g , approaching the opposite regime of non-interacting particles. On the other hand, if g is fixed, the healing length is smaller for haloes of higher mean density. Let us define the characteristic coupling strength for which $R = \xi$, therefore, as g_H , given by

$$g_H \equiv \frac{\hbar^2}{2\bar{\rho}R^2} = \frac{2}{3}\pi\hbar^2 \frac{R}{M}, \quad (40)$$

where g_H is determined by the mean density and radius (or mass and mean radius) of the halo. In later sections, it will be convenient to describe dimensionless BEC particle parameters, and so already here we define the quantities

$$y \equiv \frac{m}{m_H} \text{ and } x \equiv \sqrt{\frac{g}{g_H}} = \frac{R}{\xi}. \quad (41)$$

Thus, the BEC self-interaction regime can also be determined by the ratio of g/g_H .

Let us investigate this in more detail: In the TF-regime, the quantum-mechanical pressure in (14) is neglected. In order to see for which part of the BEC parameter space this regime can be expected to be a good approximation, we estimate the respective forces associated with the quantum-pressure term and the self-interaction term in (14), respectively. Both depend on the halo density profile's varying on a length scale of order R . Using (16), the force due to quantum pressure is estimated by

$$-\rho \nabla Q \sim \frac{\hbar^2}{2m^2} \frac{\rho}{R^3}, \quad (42)$$

while the force due to the self-interaction is of order

$$-\nabla P_{SI} \sim -\frac{g\rho^2}{2m^2 R}. \quad (43)$$

The ratio of the two becomes

⁷ Since the diluteness condition implies $n^{-1/3} \ll \xi$, one should consider the limit $R/\xi \rightarrow \infty$, rather than $\xi \rightarrow 0$.

$$\frac{|-\rho \nabla Q|}{|-\nabla P_{SI}|} \sim \frac{\hbar^2}{g \rho R^2} \sim 2 \frac{g_H}{g} \quad (44)$$

by using the definition of g_H . We see that for the above ratio to be much smaller than one, we require that

$$\frac{g}{g_H} \gg 2, \quad (45)$$

which is thus the condition for the TF regime to be valid. If we go back to the characteristic size of a spherical halo in (37), we can furthermore see that, if we set $v = v_{vir}$ in (21), we can rewrite

$$R_0 \simeq \frac{\sqrt{3}\pi^{1/4}}{12} \left(\frac{g}{g_H} \right)^{1/2} \lambda_{deB}, \quad (46)$$

from which follows $R_0/\lambda_{deB} \gg 1$ if $(g/g_H)^{1/2} = R_0/\xi \gg 1$. Therefore, in contrast to *Regime I*, λ_{deB} is much smaller than the size of the halo. However, using (41), we see that $\lambda_{deB} \simeq 4.3\xi$ in this regime, so the de-Broglie wavelength is still larger than the healing length. In *Section 3*, we will apply the Virial theorem to ellipsoidal BEC haloes in the TF regime, and we will see that this enforces the particle parameters m and g to be related according to (81)-(82) and (103)-(104), respectively. In the spherical case, the dimensionless quantities (41) are then related as

$$\frac{m}{m_H} = \frac{\sqrt{15}}{4} \sqrt{\frac{g}{g_H}}. \quad (47)$$

Therefore, it follows that in the TF regime we also have $m/m_H \gg 1$. In other words, λ_{deB} can be much smaller than R and hence the particle mass m can be much larger than m_H , but only if the self-interaction is high enough.

The above characteristic units for the DM particle mass and coupling strength can be written in fiducial values as

$$m_H = 1.066 \cdot 10^{-25} \left(\frac{R}{100 \text{ kpc}} \right)^{-1/2} \left(\frac{M}{10^{12} M_\odot} \right)^{-1/2} \text{ eV}, \quad (48)$$

and

$$g_H = 2.252 \cdot 10^{-64} \left(\frac{R}{100 \text{ kpc}} \right) \left(\frac{M}{10^{12} M_\odot} \right)^{-1} \text{ eV cm}^3, \quad (49)$$

in units where $c = 1$ and $[R] = \text{kpc}$, $[M] = M_\odot$. For haloes with a size between the Milky Way ($M = 10^{12} M_\odot$, $R = 100 \text{ kpc}$) and a typical dwarf galaxy ($M = 10^{10} M_\odot$, $R = 10 \text{ kpc}$), we see that the above quantities are in the range of

$$m_H \simeq 10^{-25..-24} \text{ eV}, \quad g_H \simeq 2 \cdot 10^{-64..-63} \text{ eV cm}^3. \quad (50)$$

The two BEC dark matter regimes are schematically described in Table 1, where also some common names are listed. The latter, however, have appeared in more recent papers, even though both regimes have been studied already in earlier literature on self-gravitating bosonic matter.

To re-iterate, both regimes revisited in this section exhibit non-classical behaviour: in *Regime I*, ∇Q in equ.(14) causes the Heisenberg uncertainty principle to act on galactic scales. In *Regime II*, on the other hand, ∇P_{SI} results in $(n = 1)$ -polytropic solutions. However, the physical nature of this pressure and the so-caused "internal energy" stems from the repulsive quantum-mechanical 2-body scattering at vanishing temperature.

Table 1. BEC dark matter regimes for a halo of (mean) radius R and mass M

I	II
quantum \gg self-interaction pressure $\xi \rightarrow R$, $g \rightarrow 0$, $m \lesssim m_H = f(R, M)$	self-interaction \gg quantum pressure $\xi \ll R$, $g \gg g_H$, $m \gg m_H$, $g/m^2 = f(R)$
$R \gtrsim \lambda_{deB} \gtrsim l_{QP}$ \rightarrow grav. bound, halo core $\sim \lambda_{deB}$ no vortices "fuzzy dark matter" (free scalar-field DM)	$R = R_0 \simeq l_{SI} \gg \lambda_{deB}$ \rightarrow grav. bound, halo core $\sim R_0$ vortices favoured "repulsive/fluid dark matter" (scalar-field DM with strong, positive self-interaction)

2.3 Stationary systems and virial equilibrium

Since we are going to study the energetic stability of vortices in this paper, we will restrict ourselves to some simplified models in the forthcoming analysis: First, we will consider stationary systems and their corresponding energy, i.e. we will restrict to time-independent systems. Our second major assumption will be that haloes rotate with a *constant* angular velocity Ω about their rotation axis. This will allow us later to move into the frame co-rotating with the halo and to study stable structures in that frame.

Stationary states are described by wavefunctions of the form $\psi(\mathbf{r}, t) = \psi_s(\mathbf{r})e^{-i\mu t/\hbar}$, where μ , the GP chemical potential, is fixed by the conservation of particle number. For these states, the mass density $\rho = m|\psi_s|^2$ and, hence, the gravitational potential Φ are time-independent, while the wavefunction evolves harmonically in time. Inserting this ψ into (3) results in the time-independent GP equation with eigenvalues μ (see also *Appendix C*),

$$\left(-\frac{\hbar^2}{2m} \Delta + g|\psi_s|^2 + m\Phi \right) \psi_s = \mu \psi_s. \quad (51)$$

The time-independent part $\psi_s(\mathbf{r})$ itself can be decomposed as

$$\psi_s(\mathbf{r}) = |\psi_s|(\mathbf{r})e^{iS_s(\mathbf{r})} \quad (52)$$

with amplitude and phase both depending on position only. We will omit the subscript 's' in the forthcoming analysis. Systems obeying (51) can be studied via the corresponding GP energy functional, which is given by

$$\mathcal{E}[\psi] = \int_V \left[\frac{\hbar^2}{2m} |\nabla \psi|^2 + \frac{m}{2} \Phi |\psi|^2 + \frac{g}{2} |\psi|^4 \right] d^3 \mathbf{r}. \quad (53)$$

On the other hand, equ.(51) could have been also obtained by variation of (53) with respect to ψ (or its complex conjugate ψ^*), under the constraint (5),

$$\frac{\delta \mathcal{E}[\psi]}{\delta \psi^*} - \mu \frac{\delta}{\delta \psi^*} \int |\psi|^2 d^3 \mathbf{r} = 0, \quad (54)$$

with μ playing the role of the Lagrange multiplier. Inserting (52) into (53), the total energy can be written in a very instructive way as

$$E = K + W + U_{SI}, \quad (55)$$

where the *total* kinetic energy term K is given by

$$K \equiv \int_V \frac{\hbar^2}{2m} |\nabla \psi|^2 d^3 \mathbf{r} = \int_V \frac{\hbar^2}{2m^2} (\nabla \sqrt{\rho})^2 d^3 \mathbf{r} + \int_V \frac{\rho}{2} \mathbf{v}^2 d^3 \mathbf{r} \equiv K_Q + T, \quad (56)$$

with K_Q accounting for the quantum-kinetic energy and T for the bulk kinetic energy (rotational, internal motion, ect.) of the body. K_Q has *no* classic counterpart, and is absent in the classical figures of equilibrium studied in Chandrasekhar (1969) or in Lai, Rasio & Shapiro (1993). Also, K_Q is *neglected* whenever the Thomas-Fermi regime is employed. The other terms in (55) are simply the gravitational potential energy

$$W \equiv \int_V \frac{\rho}{2} \Phi d^3 \mathbf{r} \quad (57)$$

and the internal energy

$$U_{SI} \equiv \int_V \frac{g}{2m^2} \rho^2 d^3 \mathbf{r}, \quad (58)$$

which is determined by the particle interactions. We have defined the latter essentially as $U_{SI} = \int P_{SI} dV$ with P_{SI} the pressure due to self-interaction (17), which, in general, is *not* the total pressure given the presence of K_Q . While we call U_{SI} the internal energy, it shall be kept in mind that its origin is not due to thermal processes but solely due to the repulsive 2-body elastic scattering. The above energy contributions are those which enter the scalar Virial theorem of a rotating, *isolated* BEC halo under self-gravity,

$$2K + W + 3U_{SI} = 0. \quad (59)$$

3 BEC HALOES WITH ANGULAR MOMENTUM

In the previous section, we have reviewed halo density profiles in the absence of rotation and angular momentum. However, we expect and assume galactic haloes to have undergone tidal torquing in the early phases of their collapse, and as such, we will model them as rotating, *non-spherical* bodies. In case of a (non-rotating) sphere ($\Omega = 0$), the BEC wavefunction were real and positive. However, for non-vanishing angular velocities, $\Omega \neq 0$, superfluid currents arise. As a result, the wave function is complex and therefore has a non-trivial phase or velocity flow, respectively, even without vortices (for laboratory BEC examples see for instance the systems studied in Fetter (1974) and Recati, Zambelli & Stringari (2001)). This means, in particular, that such a system has a non-vanishing, bulk angular momentum *prior* to vortex formation, which we will want to associate with that provided by tidal torquing, and characterized by the λ -spin parameter defined in equ.(1).

So, in modelling dark matter haloes as BEC wave functions, $\psi = |\psi|e^{iS}$, their velocity information is contained in the (real) phase function $S(t, \mathbf{r})$. As long as no defect structures like vortices appear in the flow, the condensate phase is a smooth function in which case we will use the notation S_0 in the rest of the paper. The fluid velocity is generally given by $\mathbf{v} = \hbar \nabla S_0 / m$, see equ.(13), while in a frame rotating rigidly with a constant angular velocity Ω , it is given by

$\mathbf{v}' = \mathbf{v} - \Omega \times \mathbf{r}$. In *Section 4*, we will study the energetic stability of vortices, and it will turn out to be convenient to move into a frame which rotates with the figure, i.e. at an angular velocity Ω . It is this co-rotating frame we shall consider, assuming that the haloes rotate about the z -axis, such that $\Omega = (0, 0, \Omega)$.

As we have pointed out in *Section 2*, the (vortex-free) density profile of a BEC halo has a flat core, in contrast to the r^{-1} -central cusps of standard CDM. However, that equ. (3) - with or without rotation - favours a flat core over a cusp can be also seen as follows: The equilibrium matter distribution of the BEC halo in a frame rotating rigidly with constant angular velocity Ω is given by

$$-\frac{\hbar^2}{2m} \Delta' |\psi'| + \frac{\hbar^2}{2m} |\psi'| (\nabla S')^2 + (m\Phi' + g|\psi'|^2 - \mu') |\psi'| - \hbar |\psi'| \nabla S' \cdot (\Omega \times \mathbf{r}) = 0, \quad (60)$$

(see (10) and (51)) where primes will in the following denote quantities as measured in the rotating frame, and $\mu' = \text{const.}$ Inserting a cuspy test function, $|\psi'|^2 = (r')^{-\alpha}/m$ with constant exponent $\alpha > 0$, results in

$$m\Phi' + \frac{g}{m} (r')^{-\alpha} + \frac{\hbar^2}{2m} (\nabla S')^2 - \hbar \nabla S' \cdot (\Omega \times \mathbf{r}) = \mu' + \frac{\hbar^2}{2m} \frac{\alpha}{2} \left(\frac{\alpha}{2} + 1 \right) (r')^{-2}. \quad (61)$$

Calculating the associated gravitational potential Φ' to the test function by requiring that $\nabla' \Phi' = 0$ at $r' = 0$ (i.e. no net gravitational force at the centre) requires $\alpha < 1$. However, if $\alpha > 0$ and since $\mu' = \text{const.}$, one can easily show that the resulting velocity flows \mathbf{v}' would diverge in the centre, regardless of the absence of a vortex, which would contradict the irrotationality constraint. In fact, in the next section, we will study figures of revolution as halo models, whose velocity fields *prior* to vortex formation are smooth in either frame of reference.

3.1 BEC haloes as Maclaurin spheroids

3.1.1 General properties

For the sake of computational simplicity and in order to gain analytical insight, we start our analysis by considering a simple halo model, the densities and potentials of which are given by homogeneous Maclaurin spheroids, rotating uniformly with angular velocity $\Omega = (0, 0, \Omega)$. Although the BEC fluid is compressible, as described in *Section 2*, the spherical polytrope solution shows that the density only varies by a factor of about three from the centre to the surface, see (36). Hence, the assumption of a uniform density as a first approximation is more justified for BEC than for standard CDM haloes. However, homogeneous, i.e. incompressible Maclaurin spheroids are only approximate solutions of the GP equation (51). In order for our model to be in global virial equilibrium, equ.(59), in accordance with the equations of motion, we will have to find a constraint on the underlying DM particle parameters, as will be shown in the next subsection.

We denote the mass density as ρ_0 , and the semi-axes (a_1, a_2, a_3) , lying along (x, y, z) , are such that $a_1 = a_2 \equiv a > a_3 \equiv c$. The total volume of a spheroid is $V = 4\pi a^2 c / 3$,

and we will make use of its mean radius, defined as $R = (a^2 c)^{1/3}$. The gravitational potential inside the spheroidal body is given by

$$\Phi_0(r, z) = \pi G \rho_0 \times \left[(A_1(e)r^2 + A_3(e)z^2) - 2\sqrt{1-e^2}a^2 \frac{\arcsin(e)}{e} \right] \quad (62)$$

in cylindrical coordinates (r, z) (see Chandrasekhar (1969) or Binney & Tremaine (1987) for definitions and formulas, but note the difference in the sign convention of Φ_0 between the two references. We choose the convention in Binney & Tremaine (1987)). The functions A_1 and A_3 depend on the eccentricity $e = \sqrt{1 - (c/a)^2}$ of the figure. Their general definition can be found in *Appendix A*. Here, they reduce to functions in closed-form,

$$A_1(e) = A_2(e) = \frac{\sqrt{1-e^2}}{e^3} \arcsin(e) - \frac{1-e^2}{e^2}, \quad (63)$$

$$A_3(e) = \frac{2}{e^2} - \frac{2\sqrt{1-e^2}}{e^3} \arcsin(e), \quad (64)$$

and both are positive for $e \in [0, 1)$. A family of spheroids is characterized by the following relationship between angular velocity and eccentricity, the Maclaurin formula (see e.g. Binney & Tremaine (1987))

$$\tilde{\Omega} \equiv \frac{\Omega}{\Omega_G} = \sqrt{2}(A_1(e) - (1-e^2)A_3(e))^{1/2} \quad (65)$$

with Ω_G in (31). Relation (65) parametrizes the rotation via e , and $e = 0$ for $\Omega = 0$. The figure is stable only for values of e below 0.9529 (see Chandrasekhar (1969)). For our analysis, we will also need the gravitational potential and rotational kinetic energy of the homogeneous Maclaurin spheroid,

$$W = -\frac{3}{5} \frac{GM^2}{R} (1-e^2)^{1/6} \frac{\arcsin(e)}{e} \quad (66)$$

and

$$T = \frac{4\pi}{15} (1-e^2)^{-1/3} \rho_0 \Omega^2 R^5, \quad (67)$$

respectively, along with its angular momentum

$$L = |\mathbf{L}| = \sqrt{\frac{4}{5} (1-e^2)^{-1/3} T M R^2} \quad (68)$$

(see again Chandrasekhar (1969) and Binney & Tremaine (1987) for reference). The Maclaurin spheroid experiences rigid rotation only, therefore its velocity in the two frames is simply given by

$$\mathbf{v} = \boldsymbol{\Omega} \times \mathbf{r} = \sqrt{2}\Omega_G (A_1 - (1-e^2)A_3)^{1/2} (-y, x, 0), \quad (69)$$

and $\mathbf{v}' = 0$. An illustrative plot of a velocity field in the rest frame can be found in Fig.1.

3.1.2 Comparison to CDM λ -spin parameter and virial constraint

In this subsection, we aim to express the spin parameter λ in equ.(1) as a function of the halo's eccentricity only, i.e. its shape. To this end, we first rewrite

$$\lambda = \frac{L|W|^{1/2}}{GM^{5/2}} \left| \frac{E}{W} \right|^{1/2}. \quad (70)$$

According to equations (66) and (68),

$$\frac{L|W|^{1/2}}{GM^{5/2}} = \sqrt{\frac{4}{5} M (1-e^2)^{-1/3} R^2 t} \frac{|W|}{GM^{5/2}} = \frac{6}{5\sqrt{5}} \frac{\arcsin e}{e} \sqrt{t(e)}, \quad (71)$$

with the t -parameter $t \equiv T/|W|$, a measure of rotational support, given by

$$t(e) = \frac{3}{2e^2} - 1 - \frac{3\sqrt{1-e^2}}{2e \arcsin(e)}. \quad (72)$$

This relation also applies to compressible Maclaurin spheroids as has been shown in Lai, Rasio & Shapiro (1993). The Virial theorem in (59) allows us to write

$$\left| \frac{E}{W} \right|^{1/2} = t^{1/2} \left(1 + \frac{2U_{SI}}{T} \right)^{1/2}, \quad (73)$$

where we used the fact that, for a homogeneous body, $K_Q = 0$. Using now $U_{SI} = P_0 V$ with *constant* pressure P_0 and $V = 4\pi R^3/3$ according to the definition of the spheroid's mean radius R , we get for the ratio

$$\frac{2U_{SI}}{T} = \frac{2P_0 V}{|W|t} = \frac{2}{t} \frac{5}{3} \frac{e}{\arcsin(e)} (1-e^2)^{-1/6} \frac{g}{2m^2} R G V. \quad (74)$$

It remains to establish a connection between the mean radius R of the halo and the dark matter particle parameters. The 'classical', homogeneous Maclaurin spheroid, which formally is an $(n=0)$ -polytrope, has a pressure profile and its internal energy vanishes. A BEC system, on the other hand, possesses a formal "internal energy" due to the particle self-interaction (58), and its equation of state is such that the pressure is constant in case of constant density. This apparent inconsistency is due to the fact that we model the BEC halo as a homogeneous system. In order for the BEC halo to fulfil the virial theorem globally, we thus set the BEC pressure equal to the *average* pressure of the classical spheroid, i.e. the DM particle parameters must be such that the resulting halo size corresponds to the one given by the classical spheroid. Using the pressure distribution of a homogeneous, ellipsoidal equilibrium configuration,

$$P(\mathbf{r}) = \pi G \rho_0^2 [A_3 a_3^2 - A_1 x^2 - A_2 y^2 - A_3 z^2] + \frac{\rho_0}{2} \mathbf{v}^2, \quad (75)$$

we calculate $U_{SI} = \int P(\mathbf{r}) d^3 \mathbf{r}$, which, for the Maclaurin spheroid with $A_1 = A_2$, $a_1 = a_2 \equiv a$, $a_3 \equiv c$, results in

$$\int P(\mathbf{r}) d^3 \mathbf{r} = \frac{8}{15} A_3(e) (1-e^2)^{2/3} \pi^2 G \rho_0^2 R^5. \quad (76)$$

Setting this expression equal to $U_{SI} = g \rho_0^2 / (2m^2) \int d^3 \mathbf{r}$ according to (58) and solving for the mean radius R , we get

$$R = \left(\frac{15}{3A_3(e)(1-e^2)^{2/3}} \right)^{1/2} \left(\frac{K_p}{2\pi G} \right)^{1/2} \quad (77)$$

with K_p in (17). In the spherical limit, $e \rightarrow 0$, this reduces to

$$R_0 = \sqrt{\frac{15}{2}} \left(\frac{K_p}{2\pi G} \right)^{1/2}, \quad (78)$$

which is a factor of about 1.15 smaller than the radius of a spherical $(n=1)$ -polytropic halo given in (37). Equ.(77) connects the particle parameters (m, g) via K_p to the mean radius R such that *virialized* haloes fulfill a certain constraint as can be seen as follows: using the above definitions for K_p and (40)-(41), we rewrite

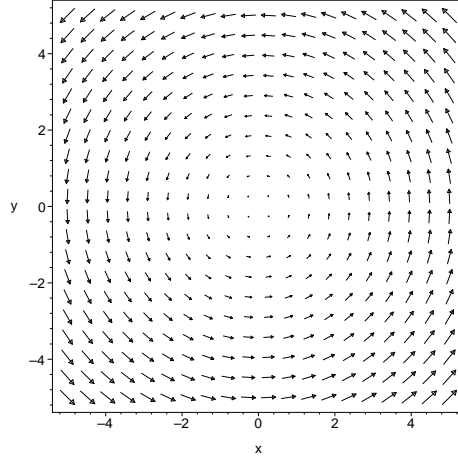


Figure 1. Illustrative velocity field of a Maclaurin spheroid in the rest frame having $\lambda = 0.05$.

$$\frac{g}{g_H} = \frac{m^2}{m_H^2} \frac{2K_p}{(g_H/m_H^2)} \quad \text{or} \quad y = \sqrt{\frac{g_H}{2K_p m_H^2}} x \quad (79)$$

and

$$\frac{g_H}{m_H^2} = \frac{\pi G}{2} R^2. \quad (80)$$

Inserting now the radius (77), we arrive at the following constraint, implied by imposing virial equilibrium,

$$y(x) = \left(\frac{5}{8A_3(e)(1-e^2)^{2/3}} \right)^{1/2} x. \quad (81)$$

The corresponding dimensional relationship is accordingly

$$m(g) = \left(\frac{5}{8A_3(e)(1-e^2)^{2/3}} \right)^{1/2} \frac{m_H}{\sqrt{g_H}} \sqrt{g}, \quad (82)$$

i.e. virialized haloes as rotating, homogeneous Maclaurin spheroids lie on a line in $(\log m, \log g)$ -space, whose slope is completely determined by the eccentricity e and the mean radius R of the halo. We will make use of this result in *Section 4*.

For now, we continue the calculation of $\lambda = \lambda(e)$. Inserting (77) into (74), we get

$$\left| \frac{E}{W} \right|^{1/2} = t^{1/2} \left(1 + \frac{e}{t} \frac{A_3(e)(1-e^2)^{1/2}}{\arcsin(e)} \right)^{1/2}. \quad (83)$$

In connection with (71), the λ -spin parameter as a function of the eccentricity e of the halo is finally given by

$$\lambda = \frac{6}{5\sqrt{5}} \frac{\arcsin e}{e} t \left(1 + \frac{e}{t} \frac{A_3(e)(1-e^2)^{1/2}}{\arcsin(e)} \right)^{1/2} \quad (84)$$

with $t = t(e)$ in (72). In our case, however, we fix λ and solve for e . In what will follow in *Section 4*, we will take three representative values, $\lambda = (0.01, 0.05, 0.1)$, which correspond to eccentricities $e = (0.062, 0.302, 0.550)$. A table of spheroid parameters as a function of λ can be found in *Appendix A*. For given values of the halo mass density and eccentricity, the angular velocity is fixed. For example, for a mean dark matter density of $1.6 \cdot 10^{-26}$ g/cm³ for the Milky-Way and $\lambda = 0.05$, we have $\Omega \sim 1.3 \cdot 10^{-17}$ rad/s, so $\Omega/\Omega_G \sim 0.22$.

The halo model presented in this subsection has the advantage of computational simplicity, however, the approximation of uniform rotation means its velocity flow is not

strictly irrotational in the rest frame as required in the absence of vortices. The approximation of uniform density, moreover, does not capture the effect of compressibility, which results from the dependence of self-interaction pressure on density in equ.(17). Therefore, we will consider a further model, which improves upon those approximations, in the next subsection.

3.2 BEC haloes as irrotational Riemann-S ellipsoids

3.2.1 General properties

In this subsection, we relieve some of the simplifying assumptions from above by allowing the density to vary in space and by imposing *strict* irrotationality in the rest frame prior to vortex formation. This will allow us to take account of the compressibility of the BEC fluid, which corresponds in the Thomas-Fermi regime to an $(n = 1)$ -polytrope (see (17)). It is possible to generalize the Maclaurin spheroids of *Section 3.1* to account for this compressibility in an approximate way, as shown by Lai, Rasio & Shapiro (1993). However, this would not allow us to impose the additional constraint of irrotationality. In general, a rotating ellipsoidal halo cannot be both axisymmetric and irrotational if it is non-singular at the origin as can be seen as follows: Suppose without lack of generality that the velocity field of the halo has the form

$$\mathbf{v} = \Omega(r, z) \times \mathbf{r} = v_\theta(r, z) \hat{\theta} = r\Omega(r, z) \hat{\theta}, \quad (85)$$

allowing for differential rotation in r and z . The corresponding vorticity is given by

$$\nabla \times \mathbf{v} = \left(-r \frac{\partial \Omega}{\partial z}, 0, \frac{1}{r} \frac{\partial}{\partial r} (r^2 \Omega) \right) \hat{\mathbf{r}}. \quad (86)$$

Requiring irrotationality $\nabla \times \mathbf{v} = 0$ is now equivalent to requiring $r^2 \Omega(r, z) = \text{constant}$ in r and $\Omega = \text{constant}$ in z . This means that either $v_\theta = \infty$ at $r = 0$ or, if at $r = 0$ we impose $v_\theta = 0$, then it follows that $\Omega(r, z) = 0$. The assumption of axisymmetry along with the constraint of ir-

rotationality lead to diverging velocity profiles in the centre of the halo or to a trivial solution⁸.

It is thus necessary to consider non-axisymmetric objects if BEC dark matter forces us to take into account the irrotationality of its velocity field along with a bulk angular momentum *prior* to vortex formation. There exists indeed a 'classical' figure of rotation which can serve this purpose, namely the irrotational Riemann-S ellipsoid. The family of Riemann-S ellipsoids with semi-axes (a_1, a_2, a_3) along (x, y, z) describes uniformly rotating bodies, as in the Maclaurin case, but with internal velocity fields *superposed*, which combine with the uniform rotation to yield a net flow with $\nabla \times \mathbf{v} = 0$, see Fig.2. Exact solutions exist for Riemann-S ellipsoids only for the case of uniform density, a limitation they share with the Maclaurin spheroids (Chandrasekhar (1969)). Fortunately, as we shall see below, Lai, Rasio & Shapiro (1993), abbreviated LRS93 in the following, developed their 'ellipsoidal approximation' also for Riemann-S ellipsoids, so we shall be able to consider the compressible case here as well⁹.

Again, we assume the uniform rotation to be about the z -axis with angular velocity Ω . The internal velocity field having angular velocity Λ is required to have its uniform vorticity parallel to Ω and to leave the ellipsoidal figure unchanged (see Chandrasekhar (1969) and *Appendix A* for more details). The mean radius of the ellipsoid is given by

$$R = (a_1 a_2 a_3)^{1/3} = a_1 (1 - e_1^2)^{1/6} (1 - e_2^2)^{1/6}, \quad (87)$$

with eccentricities

$$e_1 = \sqrt{1 - (a_2/a_1)^2} \text{ and } e_2 = \sqrt{1 - (a_3/a_1)^2}. \quad (88)$$

As in Chandrasekhar (1969) and LRS93, we write the velocity field in the frame co-rotating with the figure as

$$\mathbf{v}' = C_1 y \mathbf{x} + C_2 x \mathbf{y} \quad (89)$$

with

$$C_1 = -\frac{a_1^2}{a_1^2 + a_2^2} \zeta' = \frac{a_1}{a_2} \Lambda, \quad C_2 = \frac{a_2^2}{a_1^2 + a_2^2} \zeta' = -\frac{a_2}{a_1} \Lambda. \quad (90)$$

The vorticity in the rotating frame is defined as

$$\zeta' \equiv (\nabla' \times \mathbf{v}')_z = -\frac{a_1^2 + a_2^2}{a_1 a_2} \Lambda \equiv \Omega f_R, \quad (91)$$

and the vorticity in the rest frame is given by

$$\zeta \equiv (\nabla \times \mathbf{v})_z = \zeta' + 2\Omega = (f_R + 2)\Omega. \quad (92)$$

There is a whole class of Riemann-S ellipsoids, which differ in their value of f_R . However, only for those with $f_R = -2$ does the vorticity vanish in the rest frame, the so-called *irrotational* Riemann-S ellipsoids, and we will only consider those in the forthcoming analysis. It turns out that these ellipsoids fulfill $a_1 \geq a_2$, i.e. they are all prolate¹⁰ bodies (see Chandrasekhar (1969)). Furthermore, we can write

⁸ For fully general-relativistic, rotating boson stars, Ryan (1997) and Yoshida & Eriguchi (1997) assumed axisymmetry but in their case the velocity was singular at the centre.

⁹ As shown in LRS93, the approximate solutions for the compressible case, which result from their ellipsoidal approximation, agree well with the true equilibria.

¹⁰ As a curious note, we remark that, interestingly, recent studies on standard CDM halo formation suggest that most haloes are of prolate shape, see e.g. Plionis, Basilakos & Ragone-Figueroa

the relationship between Ω and Λ for $f_R = -2$ according to LRS93 as

$$\Omega = \frac{1}{2} \left(\frac{a_1}{a_2} + \frac{a_2}{a_1} \right) \Lambda = \frac{2 - e_1^2}{2\sqrt{1 - e_1^2}} \Lambda. \quad (93)$$

The connection between angular velocity and axis ratios or eccentricities, respectively, can again be stated in a concise form as in (65). We take the formula from LRS93 for $f_R = -2$,

$$\begin{aligned} \tilde{\Omega} \equiv \frac{\Omega}{\Omega_G} &= \left(\frac{2B_{12}}{q_n} \right)^{1/2} \left(1 + \frac{4a_1^2 a_2^2}{(a_1^2 + a_2^2)^2} \right)^{-1/2} = \\ &= \left(\frac{2B_{12}}{q_n} \right)^{1/2} \left(1 + \frac{4(1 - e_1^2)}{(2 - e_1^2)^2} \right)^{-1/2}, \end{aligned} \quad (94)$$

with $B_{12} = A_2 - a_1^2(A_1 - A_2)/(a_2^2 - a_1^2)$ and the constant q_n , depending on the polytropic index n , can be found in (A11) in *Appendix A*. In what follows, we will again take advantage of formulae which have been derived in LRS93. These are again quantities entering the Virial theorem: the gravitational potential energy

$$W = -\frac{3}{5-n} \frac{GM^2}{R} f(e_1, e_2) \quad (95)$$

with

$$\begin{aligned} f(e_1, e_2) &= \frac{1}{2} \left(A_1(1 - e_1^2)^{-1/3}(1 - e_2^2)^{-1/3} + \right. \\ &\quad \left. + A_2(1 - e_1^2)^{2/3}(1 - e_2^2)^{-1/3} + A_3(1 - e_1^2)^{-1/3}(1 - e_2^2)^{2/3} \right) \end{aligned} \quad (96)$$

and A_1, A_2, A_3 as in *Appendix A*. Furthermore, we will need the total angular momentum

$$\mathbf{L} = \frac{\kappa_n}{5} M (\Omega(a_1^2 + a_2^2) - 2a_1 a_2 \Lambda) \hat{\mathbf{z}} \quad (97)$$

and the rotational kinetic energy

$$T = \frac{\kappa_n}{20} M (a_1 - a_2)^2 (\Omega + \Lambda)^2 + \frac{\kappa_n}{20} M (a_1 + a_2)^2 (\Omega - \Lambda)^2, \quad (98)$$

with κ_n being another constant depending on the polytropic index n (see A10). Neglecting the quantum pressure by restricting to the Thomas-Fermi regime will amount to setting $n = 1$ in the above formulae.

The irrotational Riemann-S ellipsoid experiences an internal motion on top of the rigid rotation. Using (89) - (94), its velocity field in the rotating frame can be derived as

$$\begin{aligned} \mathbf{v}' &= \frac{2}{2 - e_1^2} \Omega (y, -(1 - e_1^2)x, 0) = \\ &= 2\Omega_G \left(\frac{2B_{12}}{q_n} \right)^{1/2} (8(1 - e_1^2) + e_1^4)^{-1/2} (y, -(1 - e_1^2)x, 0), \end{aligned} \quad (99)$$

while the velocity in the rest frame is accordingly

$$\begin{aligned} \mathbf{v} &= \mathbf{v}' + \Omega \times \mathbf{r} = \Omega \frac{e_1^2}{2 - e_1^2} (y, x, 0) = \\ &= \Omega_G \left(\frac{2B_{12}}{q_n} \right)^{1/2} (1 + 8(1 - e_1^2)/e_1^4)^{-1/2} (y, x, 0). \end{aligned} \quad (100)$$

(2006) and Gottlöber & Yepes (2007). The reason there, however, is to be found in details of the tidal interactions, and not the constraint of irrotationality.

Both expressions depend on the polytropic index n via q_n . Illustrative plots can be found in Fig.2. Note that the limit $e_1 = 0$, $e_2 \equiv e$ does *not* reduce to the Maclaurin spheroid case. Instead, the irrotational Riemann-S sequence bifurcates from the non-rotating sphere. However, the sphere considered as the first member of the irrotational sequence is viewed from a frame rotating with angular velocity Ω , which can be explicitly seen by setting $e_1 = 0$ in the above expressions for the velocity, resulting in $\mathbf{v} = \mathbf{0}$ and $\mathbf{v}' = -\Omega \times \mathbf{r}$ (see also LRS93 and their equ.(5.5) and (5.6), which reduce to $L = 0$ and $T = 0$, hence $\mathbf{v} = \mathbf{0}$ in that case).

3.2.2 Comparison to CDM λ -spin parameter and virial constraint

In what will follow in the next section, we will also use the Riemann-S ellipsoid as a model for rotating haloes in the Thomas-Fermi regime. The condition of Virial equilibrium relates the values of $y = m/m_H$ and $x = \sqrt{g/g_H}$ then to $(n = 1)$ -polytropes. For the general case of rotating haloes, we use again (79) and (80) along with formula (3.25) of LRS93, which relates the mean radius R of the ellipsoid to the radius R_0 of the equilibrium spherical polytrope, equ.(37). For $(n = 1)^{11}$, that formula becomes

$$R = R_0[f(e_1, e_2)(1 - 2t)]^{-1/2} \equiv R_0 g(e_1, e_2)^{-1/2}, \quad (101)$$

where the t -parameter and $g \equiv f(1 - 2t)$ depend on the eccentricities of the rotating figure only,

$$t(e_1, e_2) = \frac{\kappa_1}{5} \tilde{\Omega}^2 (1 - e_1^2)^{-1/3} (1 - e_2^2)^{-1/3} \times \\ \times \left[\frac{1}{2} (2 - e_1^2) - \frac{4(1 - e_1^2)}{2 - e_1^2} + \frac{8(1 - e_1^2)^2}{(2 - e_1^2)^3} \right] |f(e_1, e_2)|^{-1} \quad (102)$$

with $\tilde{\Omega}$ from (94), $f(e_1, e_2)$ in (96) and κ_1 in (A10). Inserting (101) into (80) and the result back into (79) yields the Virial constraint

$$y(x) = \frac{\pi}{\sqrt{8}} g(e_1, e_2)^{-1/2} x, \quad (103)$$

with corresponding dimensional form

$$m(g) = \frac{\pi}{\sqrt{8}} g(e_1, e_2)^{-1/2} \frac{m_H}{\sqrt{g_H}} \sqrt{g}, \quad (104)$$

depending again only on the eccentricities (e_1, e_2) and mean radius R of the halo. Equ. (103) and (104) are the equivalent relations to (81) and (82), constraining the BEC dark matter particle parameters such that rotating haloes as irrotational Riemann-S ellipsoids in the Thomas-Fermi regime fulfill virial equilibrium. Their formal equality does not come as a surprise, since the assumption of homogeneity in *Section 3.1.2* results in the same neglect of K_Q in (59) as in the Thomas-Fermi regime (albeit the latter does not neglect the spatial variation of the density, even though its Laplacian is likewise disregarded, as in the homogeneous case).

As in *Section 3.1.2*, we shall now also derive a relation between the spin parameter λ and the eccentricities of

the ellipsoid (e_1, e_2) . Using (95), (97) and (98) for $n = 1$, the corresponding ratio $2U_{SI}/T$ in (73) is here given by

$$\frac{2U_{SI}}{T} = \frac{2U_{SI}}{|W|t} = \\ = \frac{4}{3t} \frac{g\rho_c^E}{2m^2} \frac{R}{GM} |f(e_1, e_2)|^{-1} = \frac{2}{3t} g(e_1, e_2)^{-1/2} f(e_1, e_2)^{-1}, \quad (105)$$

and we have also used (101) and (37). ρ_c^E denotes the central density of the ellipsoid. After some more algebra, we finally arrive at

$$\lambda = \frac{3\kappa_1}{20} (1 - e_1^2)^{-1/3} (1 - e_2^2)^{-1/3} (2 - e_1^2) \left(1 - \frac{4(1 - e_1^2)}{(2 - e_1^2)^2} \right) \times \\ \times |f(e_1, e_2)|^{1/2} \tilde{\Omega} \left(t + \frac{2f(e_1, e_2)^{-3/2}}{3(1 - 2t)^{1/2}} \right)^{1/2} \quad (106)$$

with $\tilde{\Omega}$ in (94) and t in (102). We use this equation, along with (A9), in order to solve for the eccentricities (e_1, e_2) at given λ . Although highly nonlinear, involving many trigonometric and elliptic functions, equ.(106) can be solved, in principle, as straightforwardly as the much simpler relationship (84). The same values of $\lambda = (0.01, 0.05, 0.1)$ as in the previous section correspond now to eccentricities of $(e_1, e_2) = (0.707, 0.573)$, $(e_1, e_2) = (0.881, 0.797)$ and $(e_1, e_2) = (0.934, 0.887)$, respectively. Note that even for small λ -values, the eccentricities are quite large, and surpass those in the case of the homogeneous spheroid. This is in part due to the fact that compressible bodies allow for higher eccentricities at a given angular momentum than incompressible ones do. A table of ellipsoid parameters as a function of λ can be found in *Appendix A*.

4 INSTABILITY OF ROTATING BEC HALOES TO VORTEX FORMATION

4.1 Energy argument

We shall use an energy argument in order to derive the critical angular velocity and energy for vortex creation in a rotating, self-gravitating BEC halo. Configurations rotating at an angular velocity Ω in the rest frame will be stationary solutions in the co-rotating frame. Therefore, we seek for vortex solutions which are (energetically) stable in the rotating frame. To this aim, we will compare the total energy with and without a vortex as measured in this frame. The equation of motion in the rotating frame is given by equ.(3) with an additional operator $V_{rot} = -\Omega \cdot \mathbf{L}'$ on the right-hand-side under the brackets with angular momentum $\mathbf{L}' = -i\hbar \mathbf{r}' \times \nabla'$, and it is also understood that the primed variables and quantities are then those in the rotating frame. The GP energy functional is then

$$\mathcal{E}'[\psi'] = \int_V \left[\frac{\hbar^2}{2m} |\nabla' \psi'|^2 + \frac{m}{2} \Phi |\psi'|^2 + \frac{g}{2} |\psi'|^4 - \right. \\ \left. - i\hbar \psi'^* \nabla' \psi' \cdot (\Omega \times \mathbf{r}') \right] d^3 \mathbf{r}'. \quad (107)$$

In what follows, we shall use (107) to determine at which energy or angular velocity respectively, the presence of a vortex starts to be energetically favoured, and to derive the vortex energy as a function of the dark matter particle parameters.

¹¹ For $(n = 0)$, their formula (3.25) reduces to $R = R_0$. However, it would not have been correct to use this result for the BEC haloes we were considering in Section 3.1. due to our matching of the BEC pressure with the average pressure of an homogeneous spheroid, and so we needed to derive (77).

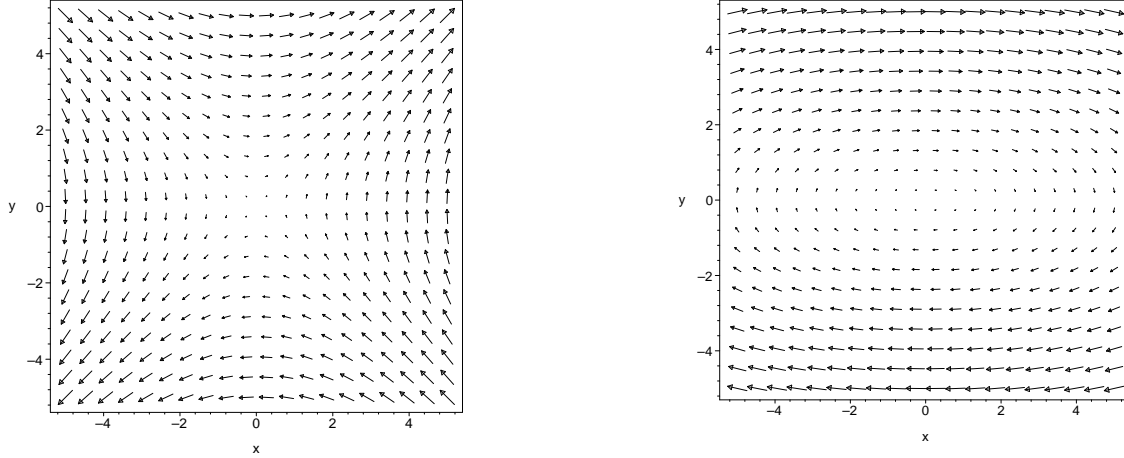


Figure 2. Illustrative velocity fields of an irrotational Riemann-S ellipsoid with $n = 1$ and $\lambda = 0.05$ in the rest frame (*left-hand-plot*) and in the co-rotating frame (*right-hand-plot*).

We will refer to a system without vortices (thus prior to vortex formation) as the unperturbed system with $\psi'_0 = f'e^{iS'_0}$, and the unperturbed (vortex-free) halo density $|\psi'_0|^2 = |f'|^2 = |f|^2$. The associated halo mass density and gravitational potential will be denoted as $\rho_0 = m|f|^2$ and Φ_0 , respectively. The corresponding phase S'_0 has no singularity in that case. These unperturbed haloes will be modelled by the ellipsoidal figures described in the previous section. However, before we turn our attention to the energy analysis, we highlight a necessary condition for vortex existence.

4.2 Necessary minimum condition for vortex formation $L \geq L_{QM}$

Applying a rotation with small enough, finite angular velocity to a perfectly *spherical-symmetric* BEC does not elevate its angular momentum above zero. It is only above a critical value Ω_c , when a (singly-quantized) vortex starts to form, that the total angular momentum is given by the amount necessary to sustain this vortex, $L_{QM} = N\hbar$. However, non-spherical bodies carry already a bulk angular momentum prior to vortex formation which is responsible for their deformation, i.e. L grows with Ω even for $\Omega < \Omega_c$ (a very illustrative plot of such an $L - \Omega$ relationship can be found in Fetter (1974)). We can easily derive a relationship between the angular momentum L of our ellipsoidal haloes and the minimum angular momentum L_{QM} necessary to sustain one vortex. In dividing equ.(68) by L_{QM} we have for the Maclaurin spheroid

$$\frac{L}{L_{QM}} = \frac{m}{\hbar M} \frac{2}{5} (1 - e^2)^{-1/3} MR^2 \Omega = \frac{2}{5} (1 - e^2)^{-1/3} \frac{m}{m_H} \frac{\Omega}{\Omega_G}$$

and by using (65),

$$\frac{L}{L_{QM}} = \frac{m}{m_H} \frac{2\sqrt{2}}{5(1 - e^2)^{1/3}} \sqrt{A_1(e) - (1 - e^2)A_3(e)}. \quad (108)$$

The equivalent relationship for the irrotational Riemann-S ellipsoid using (97) and (94) is

$$\frac{L}{L_{QM}} = \frac{m}{m_H} \frac{\kappa_n}{10} \frac{2\tilde{\Omega}\sqrt{1 - e_1^2}e_1^4}{(2 - e_1^2)(1 - e_1^2)^{5/6}(1 - e_2^2)^{1/3}}$$

$$= \frac{m}{m_H} \frac{\kappa_n}{10} \times \left(\frac{2B_{12}}{q_n} \right)^{1/2} \left(2 + \frac{e_1^4}{4(1 - e_1^2)} \right)^{-1/2} \frac{e_1^4}{(1 - e_1^2)^{5/6}(1 - e_2^2)^{1/3}}. \quad (109)$$

This shows that for fixed eccentricities (and fixed polytropic index in equ.(109)), the amount of angular momentum (in units of L_{QM}) of haloes depends only on the BEC-CDM particle mass (in units of m_H). That means that for a given shape of the halo, the amount of angular momentum necessary to sustain a vortex depends on the particle mass, such that only above a critical mass has the system enough angular momentum to sustain the vortex. At higher masses, even more angular momentum than needed can be provided. We show in Fig.3, left-hand-plot, the ratio m/m_H as a function of λ for the two figures considered in this paper, for respective values of $L/L_{QM} = 1, 10, 100$. The lowest curve, $L = L_{QM}$, establishes a lower bound on the particle mass for a given halo's λ -value for vortex existence. We also show m/m_H as a function of L/L_{QM} for fixed $\lambda = (0.01, 0.05, 0.1)$ (Fig.3, right-hand-plot). For a given L/L_{QM} , a higher particle mass for vortex formation is required for haloes with smaller spin-parameter.

However, no bounds on the other BEC particle parameter, the self-interaction strength g/g_H , can be determined from these arguments, and only the energy analysis of the next subsection will provide us with a sufficient condition on vortex formation, constraining g/g_H to be larger than a critical value $(g/g_H)_{crit}$ for a given particle mass m/m_H , as we will show.

We will now investigate vortex formation for the two models for rotating haloes described in *Section 3*: *Halo-Model A* is referred to a halo which has much more angular momentum than the minimum condition requires, $L \gg L_{QM}$. Since this is a regime which can mimic solid-body rotation, we will use the Maclaurin spheroid figures of *Section 3.1*. The other model, *Halo-Model B*, has only enough angular momentum to support a single vortex, i.e. the vortex takes up all of the angular momentum, once it has formed. The underlying halo will be modelled by the irrotational Riemann-S ellipsoids of *Section 3.2* in this case.

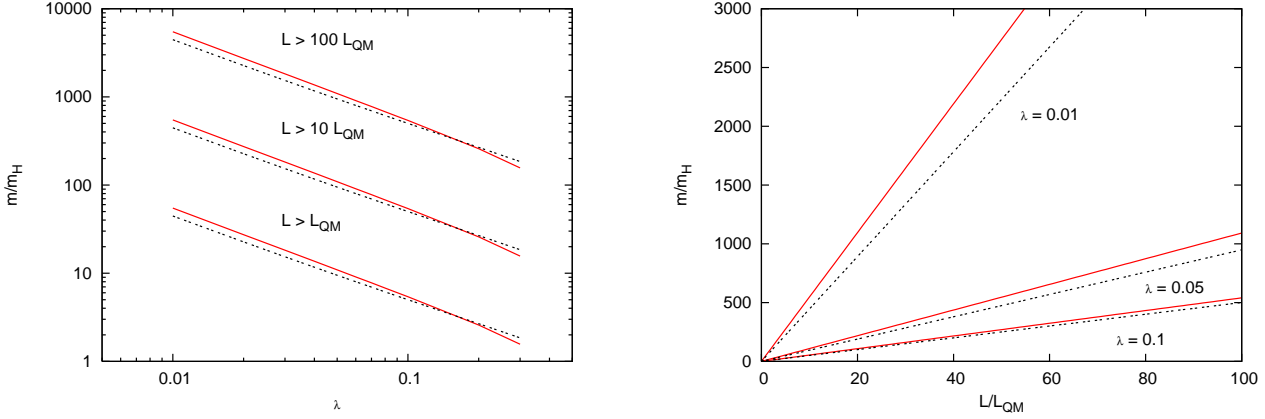


Figure 3. Dimensionless BEC-CDM particle mass m/m_H and halo angular momentum: *Left-hand-plot:* m/m_H versus λ -spin parameter for homogeneous Maclaurin spheroids (solid) and $(n = 1)$ -polytropic, irrotational Riemann-S ellipsoids (dashed) having $L/L_{QM} = 1, 10, 100$ (lower to upper curves). *Right-hand-plot:* m/m_H versus L/L_{QM} for $\lambda = 0.01, 0.05, 0.1$ for Maclaurin spheroids (solid) and Riemann-S ellipsoids (dashed).

4.3 Halo-Model A: $L \gg L_{QM}$

4.3.1 Energy splitting and vortex ansatz for the Maclaurin spheroid

For brevity, we will omit the primes on variables in the forthcoming sections *except* for the phase functions and energies in order to avoid a confusion between rotating and rest frames. In order to pursue the energy analysis, we will decompose the halo wave function ψ into a vortex-free part, $\psi_0 = f e^{iS'_0}$, and a vortex part, $w = |w| e^{iS'_1}$, according to

$$\psi = |\psi| e^{iS'} = \psi_0 w = f |w| e^{i(S'_0 + S'_1)}, \quad (110)$$

where the corresponding amplitude $|\psi| = f|w|$ is a product state of unperturbed (vortex-free) and perturbed (vortex-carrying) parts, while the contributions in the phase are additive, $S' = S'_0 + S'_1$. We will insert this ansatz for the perturbed dark matter halo into the energy functional in equ. (107). This will lead to a convenient splitting of the energy contributions, allowing us to compare them more easily. As a prerequisite, we note that for vortex-free haloes, equ. (10) and (11) in the rotating frame are

$$\begin{aligned} \Delta f - f(\nabla S'_0)^2 - \frac{2m}{\hbar^2} f(m\Phi + g f^2 - \mu) + \\ + \frac{2m}{\hbar} f \nabla S'_0 \cdot (\Omega \times \mathbf{r}) = 0 \end{aligned} \quad (111)$$

and

$$\nabla \cdot \left[f^2 \left(\nabla S'_0 - \frac{m}{\hbar} \Omega \times \mathbf{r} \right) \right] = 0 \quad (112)$$

where μ is the associated chemical potential to the normalization $\int_V f^2 = N = \int_V |\psi|^2$. The corresponding energy functional for unperturbed haloes is given by

$$\begin{aligned} \mathcal{E}'[f e^{iS'_0}] = \int_V \left\{ \frac{\hbar^2}{2m} (\nabla f)^2 + f^2 \left(\frac{m}{2} \Phi + \frac{g}{2} f^2 \right) + \right. \\ \left. + \frac{\hbar^2}{2m} f^2 \nabla S'_0 \cdot \left(\nabla S'_0 - \frac{2m}{\hbar} \Omega \times \mathbf{r} \right) \right\} d^3 \mathbf{r}. \end{aligned} \quad (113)$$

We refer the reader to *Appendix B* for the derivation of the energy splitting. It is shown there that for ψ in (110), the associated Gross-Pitaevskii energy can be written as

$$\mathcal{E}'[\psi] = \mathcal{E}'[f e^{iS'_0}] + \mathcal{G}'_f[w] - \mathcal{R}'_f[w] \quad (114)$$

with $\mathcal{E}'[f e^{iS'_0}]$ in (113),

$$\begin{aligned} \mathcal{G}'_f[w] \equiv \int \left(\frac{\hbar^2}{2m} f^2 |\nabla w|^2 + \frac{g}{2} f^4 (1 - |w|^2)^2 \right) d^3 \mathbf{r} + \\ + \int \left(\frac{m}{2} f^2 \Phi_0 + \frac{m}{2} f^2 |w|^2 [\Phi - 2\Phi_0] \right) d^3 \mathbf{r} \end{aligned} \quad (115)$$

and

$$\mathcal{R}'_f[w] \equiv \frac{\hbar^2}{m} \int i f^2 w^* \nabla w \cdot \left(\nabla S'_0 - \frac{m}{\hbar} \Omega \times \mathbf{r} \right) d^3 \mathbf{r}. \quad (116)$$

The terms apart from $\mathcal{E}'[f e^{iS'_0}]$ describe the contribution of vortices to the energy. So, using the decomposition (110) vortices of ψ (if present) are vortices of w and they are described via the energy functionals $\mathcal{G}'_f[w] - \mathcal{R}'_f[w]$ in (114). A similar splitting was deduced in Aftalion & Du (2001) and Rindler-Daller (2008) for laboratory BECs in the Thomas-Fermi regime $R/\xi \gg 1$. However, it can be easily seen that this splitting holds for any values of $R/\xi \geq 1$. There is, however, a notable change in the form of an additional term in $\mathcal{G}'_f[w]$ which stems from the fact that the external trap for atomic gases is replaced here by the gravitational potential, which depends on the density profile via Poisson's equation and is hence affected by the presence of vortices. For laboratory BECs, on the other hand, the trap potential is fixed from the outset by the adopted laser configuration, and $\mathcal{G}'_f[w]$ does not contain the potential explicitly.

We want to determine the critical angular velocity and energy above which at least one vortex in the halo will form. In order to derive an analytical result and to be as general as possible in the same time, we will consider a d -quantized straight, axisymmetric vortex, along the rotation-axis with core radius s . This core radius is given by that (cylindrical) radius, where the density recovers back from the inner vortex profile to its unperturbed bulk value. The most general ansatz for the wavefunction of such a vortex is $w = |w|(r) e^{i d \phi}$, where the modulus depends only on the radial variable. Inserting this ansatz into the Gross-Pitaevskii equation, one may solve numerically for the density profile of the halo in the presence of a vortex. However, it can

be shown that for gravitational potentials Φ falling off as $-1/r^b$, $b \leq 2$ at infinity¹², this profile goes like $r^{|d|}$ for $r \rightarrow 0$, after imposing the constraint that it approaches the unperturbed density for $r \rightarrow \infty$. This is the well-known behaviour valid also for trap potentials used in atomic BEC gases. So, the density of the halo will tend to zero towards the axis of the vortex. For our purposes, it will be sufficient to catch this behaviour by the simpler profile we are going to adopt. Our ansatz for the vortex is

$$\tilde{w}(r, \phi) = |\tilde{w}|(r)e^{iS'_1} \quad (117)$$

with amplitude

$$|\tilde{w}|(r) = \begin{cases} 1 & \text{for } r \geq s \\ C_n \left(\frac{r}{s}\right)^d & \text{otherwise} \end{cases} \quad (118)$$

and phase $S'_1 = d\phi$. This amplitude reflects the fact that outside of the vortex, the halo (number) density is given by the unperturbed profile $|f|^2 = \rho_0/m$. Since \tilde{w} is going to be multiplied by the unperturbed wave function according to the above decomposition (110), $\tilde{\psi} = \psi_0 \tilde{w}$, its amplitude is dimensionless and the z -dependence is trivial for the straight vortex. We think that the consideration of a bent vortex will not change our conclusions given the orders of magnitudes involved in the final results. The constant C_n is determined by the normalization $\int |\tilde{\psi}|^2 = N$. Although the mass is conserved, the above ansatz for the vortex causes an unnatural steepening or 'overshooting' of the profile at the core radius, which would cause a singularity in the dynamical equations. However, this feature is invisible to the energy calculation we are going to perform.

The vortex changes the gravitational potential of the smooth, vortex-free halo (62). Owing to the linearity of the Poisson equation, we may decompose the total halo potential and mass density into unperturbed and perturbed parts,

$$\Phi = \Phi_0 + \Phi_1, \quad \rho = \rho_0 + \rho_1,$$

where Φ_1 is the associated potential to the perturbation of the density due to the vortex,

$$\rho_1 = \rho - \rho_0 = \rho_0(|\tilde{w}|^2 - 1) = \begin{cases} 0 & \text{outside the vortex} \\ \rho_0 \left(C_n^2 \left(\frac{r}{s}\right)^{2d} - 1\right) < 0 & \text{otherwise} \end{cases} \quad (119)$$

according to (117), and $\Delta\Phi = \Delta\Phi_0 + \Delta\Phi_1 = 4\pi G(\rho_0 + \rho_1)$. So, we are left to solve for the unknown potential of the vortex configuration,

$$\Delta\Phi_1 = 4\pi G\rho_1 = \begin{cases} 0 & \text{outside the vortex} \\ 4\pi G\rho_0 \left(C_n^2 \left(\frac{r}{s}\right)^{2d} - 1\right) < 0 & \text{otherwise.} \end{cases} \quad (120)$$

The first case amounts simply to solving the Laplace equation, while the second case is an inhomogeneous extension. Since we only encounter axisymmetric configurations, both cases can be solved analytically. However, since the solution for $d > 1$ happens to be a very cumbersome expression involving numerous hypergeometric functions, we will in the forthcoming analysis restrict our attention to singly-quantized vortices having $d = 1$, whose corresponding profile

can be found in Fig.4. In fact, physical reasoning makes the ($d = 1$)-vortex more interesting, since multiply-quantized vortices are generally subject to splitting into several singly-quantized vortices. The above differential equations (120) can be solved in a standard way, and the subtle issue remaining is the choice of suitable boundary conditions. For the outer-vortex solution, we impose that the potential approaches a point-mass potential for large r at fixed z , or large z at fixed r , respectively, resulting into

$$\Phi_1^{(o)}(r, z) = \frac{2\pi G\rho_0 c s^2}{\sqrt{r^2 + z^2}}. \quad (121)$$

For the inner-vortex solution, we require the gradient of the potential to vanish, i.e. no net gravitational force, at the centre, resulting in

$$\Phi_1^{(i)}(r, z) = \pi G\rho_0 r^2 \left(\frac{1}{2} \left(\frac{r}{s} \right)^2 - 1 \right). \quad (122)$$

The total halo potential in the presence of this vortex is then given by

$$\Phi = \begin{cases} \Phi_0 + \Phi_1^{(o)} & \text{outside the vortex} \\ \Phi_0 + \Phi_1^{(i)} & \text{otherwise} \end{cases} \quad (123)$$

with the potentials given in (62), (121) and (122).

In *Halo-Model A*, the vortex is essentially considered to be a perturbation of the total angular momentum L of the halo. Since the latter is conserved, that part carried by the vortex, L_{QM} , is assumed to be small compared to L , such that the total angular momentum of the system before and after vortex formation can be given by L in (68).

4.3.2 Vortex energy and critical angular velocity

Our prescription for the halo wave function is thus $\tilde{\psi} = \psi_0 \tilde{w}$ with the unperturbed wave function $\psi_0 = f e^{iS'_0}$ having the above described geometry and rotational properties of the Maclaurin spheroid and the vortex ansatz \tilde{w} from (117). The normalization constant is then $C_n = \sqrt{d+1}$. Inserting this wave function ansatz into equ.(114) will give us the critical angular velocity Ω_c above which the energy is lowered by the presence of that vortex. Since our ansatz leads to an energy greater than that which would result if the 'real' wave function were used in place of the ansatz, this means vortex creation is energetically favoured, in general, if $\Omega > \Omega_c$. More precisely, we have the upper bound

$$\begin{aligned} \mathcal{E}'[\psi] &\leq \mathcal{E}'[\tilde{\psi}] = \mathcal{E}'[f e^{iS'_0}] + \mathcal{G}'_f[\tilde{w}] - \mathcal{R}'_f[\tilde{w}] = \\ &= \mathcal{E}'[f e^{iS'_0}] + \int \left(\frac{\hbar^2}{2m} f^2 |\nabla \tilde{w}|^2 + \frac{g}{2} f^4 (1 - |\tilde{w}|^2)^2 + \right. \\ &\quad \left. + \frac{\rho_0}{2} \Phi_0 (1 - |\tilde{w}|^2) + \frac{\rho_0 |\tilde{w}|^2}{2} \Phi_1 \right) d^3 \mathbf{r} - \\ &\quad - \frac{\hbar^2}{m} f^2 \int i \tilde{w}^* \nabla \tilde{w} \cdot \left(\nabla S'_0 - \frac{m}{\hbar} \boldsymbol{\Omega} \times \mathbf{r} \right) d^3 \mathbf{r}. \end{aligned} \quad (124)$$

Since $|f|^2 = \rho_0/m$, is constant, the integrals can be performed straightforwardly. Furthermore, $\nabla S'_0 = 0$ since the spheroid has no net velocity in the rotating frame, $\mathbf{v}' = \mathbf{0}$. Let us consider each term separately, where we split the axisymmetric integration domain according to our ansatz: the quantum-kinetic term is affected by the presence of the vortex, so

¹² More precisely, we require that if $O(\mu - \Phi) \sim 1/r^b$, then $b \leq 2$.

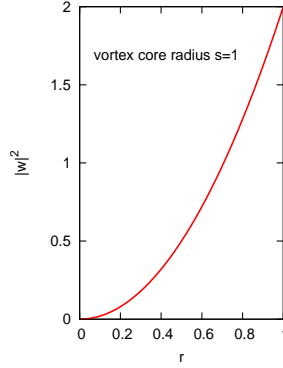


Figure 4. (Number) density profile of the vortex ansatz of equ.(118) for $d = 1$.

$$\begin{aligned}
 & \int \frac{\hbar^2}{2m} f^2 |\nabla \tilde{w}|^2 d^3 \mathbf{r} = \\
 & = \frac{\hbar^2}{2m} f^2 \int_{z=-c}^c \int_0^{2\pi} \int_{r=s}^a \sqrt{1 - \frac{z^2}{c^2}} |\nabla \tilde{w}|^2 r dr dz d\phi + \\
 & + \frac{\hbar^2}{2m} f^2 \int_{z=-c}^c \int_0^{2\pi} \int_{r=0}^s |\nabla \tilde{w}|^2 r dr dz d\phi = \\
 & = \frac{2\pi c f^2 \hbar^2 d^2}{m} \left[\ln \frac{a}{s} + \ln 2 - 1 + \frac{d+1}{d} \right], \quad (125)
 \end{aligned}$$

where the leading logarithmic term stems from the angular kinetic energy of the vortex. The term due to the self-interaction amounts to

$$\int_{-c}^c \int_0^{2\pi} \int_0^s \frac{g}{2} f^4 (1 - |\tilde{w}|^2)^2 r dr d\phi dz = g f^4 \pi c s^2 \frac{d^2}{2d+1}, \quad (126)$$

while the rotation term becomes

$$\begin{aligned}
 \mathcal{R}'_f[\tilde{w}] &= \hbar f^2 \int_{-c}^c \int_0^{2\pi} \int_0^a \sqrt{1 - \frac{z^2}{c^2}} i \tilde{w}^* \nabla \tilde{w} \cdot (\boldsymbol{\Omega} \times \mathbf{r}) r dr d\phi dz = \\
 &= \frac{4}{3} \pi \hbar f^2 c a^2 d \Omega. \quad (127)
 \end{aligned}$$

Inserting (121) - (123) and (62) into the second integral of (115), the gravitational potential energy due to the ($d = 1$)-vortex perturbation is finally given by

$$\begin{aligned}
 & \int_{-c}^c \int_0^{2\pi} \int_s^a \sqrt{1 - \frac{z^2}{c^2}} \frac{\rho_0}{2} \Phi_1^{(o)} r dr d\phi dz + \\
 & + \int_{-c}^c \int_0^{2\pi} \int_0^s \left[\frac{\rho_0}{2} \Phi_0 \left(1 - C_N^2 \left(\frac{r}{s} \right)^{2d} \right) + \right. \\
 & \left. + \frac{\rho_0}{2} C_N^2 \left(\frac{r}{s} \right)^{2d} \Phi_1^{(i)} \right] r dr d\phi dz = \\
 & = 2\pi^2 G \rho_0^2 c s^2 \left[c^2 + \frac{ac}{e} \arcsin(e) - c^2 \sqrt{1 + \left(\frac{s}{c} \right)^2} - \right. \\
 & \left. - s^2 \ln \left(\frac{c}{s} + \sqrt{\left(\frac{c}{s} \right)^2 + 1} \right) \right] - \frac{\pi^2 G \rho_0^2}{6} s^4 c (A_1(e) + 5/2). \quad (128)
 \end{aligned}$$

The above terms constitute the total energy $\mathcal{E}'[\tilde{w}]$ of our ansatz for the wave function $\tilde{\psi} = \psi_0 \tilde{w}$. Before we collect the above terms, we set $d = 1$ everywhere and rewrite the semi-axes a and c in terms of the mean radius R and the

eccentricity e . Also, we use (30) in order to finally write the vortex energy in the rotating frame as

$$\delta E' \equiv \mathcal{G}'_f[\tilde{w}] - \mathcal{R}'_f[\tilde{w}]$$

or

$$\begin{aligned}
 & \frac{\delta E'}{\Omega_{QM} L_{QM}} = \\
 & = \frac{3}{2} (1 - e^2)^{1/3} \left[\ln \left(\frac{R}{\xi} \right) + \ln \left(2(1 - e^2)^{-1/6} \right) + \frac{13}{12} \right] + \\
 & + \frac{3}{2} \left(\frac{\Omega_G}{\Omega_{QM}} \right)^2 \left(\frac{\xi}{R} \right)^2 (1 - e^2)^{1/3} \times \\
 & \times \left[(1 - e^2)^{2/3} + \frac{\arcsin(e)}{e} (1 - e^2)^{1/6} - \right. \\
 & - \left(\frac{\xi}{R} \right) (1 - e^2)^{1/3} \sqrt{1 + \left(\frac{R}{\xi} \right)^2 (1 - e^2)^{2/3}} - \\
 & - \left(\frac{\xi}{R} \right)^2 \ln \left(\frac{R}{\xi} (1 - e^2)^{1/3} + \sqrt{1 + \left(\frac{R}{\xi} \right)^2 (1 - e^2)^{2/3}} \right) \left. \right] - \\
 & - \frac{1}{8} \left(\frac{\Omega_G}{\Omega_{QM}} \right)^2 \left(\frac{\xi}{R} \right)^4 (1 - e^2)^{1/3} \left(A_1(e) + \frac{5}{2} \right) - \frac{\Omega}{\Omega_{QM}}. \quad (129)
 \end{aligned}$$

For singly-quantized vortices, the core radius s is almost the same size than the healing length ξ (see e.g. Pitaevskii & Stringari (2003)), and can be very well approximated by it, so we have replaced s by ξ in the above expressions altogether. We have also used (39) to replace the coupling strength g by the healing length ξ .

We can rewrite the variables appearing in (129) in terms of the BEC particle parameters m and g using (28)-(31) and (40) - (41) in order to arrive at

$$\begin{aligned}
 & \frac{\delta E'}{\Omega_{QM} L_{QM}} = \\
 & = \frac{3}{2} (1 - e^2)^{1/3} \left[\ln \frac{1}{2} \left(\frac{g}{g_H} \right) + \ln \left(2(1 - e^2)^{-1/6} \right) + \frac{13}{12} \right] + \\
 & + \frac{3}{2} \left(\frac{m}{m_H} \right)^2 \frac{g_H}{g} (1 - e^2)^{1/3} \left[(1 - e^2)^{2/3} + \frac{\arcsin(e)}{e} (1 - e^2)^{1/6} - \right. \\
 & - \left(\frac{g_H}{g} \right)^{1/2} (1 - e^2)^{1/3} \sqrt{1 + \frac{g}{g_H} (1 - e^2)^{2/3}} - \left. \right]
 \end{aligned}$$

$$- \frac{g_H}{g} \ln \left(\sqrt{\frac{g}{g_H}} (1-e^2)^{1/3} + \sqrt{1 + \frac{g}{g_H} (1-e^2)^{2/3}} \right) - \frac{1}{8} \left(\frac{m}{m_H} \right)^2 \left(\frac{g_H}{g} \right)^2 (1-e^2)^{1/3} \left(A_1(e) + \frac{5}{2} \right) - \tilde{\Omega}(e) \frac{m}{m_H} \quad (130)$$

with $\tilde{\Omega}$ in (65). Now, the total energy (124) will be *lower* than the vortex-free, unperturbed energy $\mathcal{E}'[fe^{iS'_0}]$ if the vortex energy in the rotating frame $\delta E'$ becomes smaller than zero, i.e. if the system with vortex is energetically favoured. The critical condition amounts to setting $\delta E' = 0$ in (130) and finding the respective relationship between the particle parameters $y = m/m_H$, $x = \sqrt{g/g_H}$ for fixed halo eccentricity. We see that the critical curves are just the two solution branches of a quadratic equation

$$y_{1,2}(x) = b/(2a(x)) [1 \pm \sqrt{1 - 4a(x)c(x)/b^2}] \quad (131)$$

with

$$a(x) \equiv \frac{1}{x^2} \left[(1-e^2)^{2/3} + \frac{\arcsin(e)}{e} (1-e^2)^{1/6} - \frac{(1-e^2)^{1/3}}{x^2} \sqrt{1 + x^2(1-e^2)^{2/3}} - \frac{1}{x^2} \ln \left(x(1-e^2)^{1/3} + \sqrt{1 + x^2(1-e^2)^{2/3}} \right) \right] - \frac{A_1(e) + 5/2}{12} \frac{1}{x^4}, \quad (132)$$

$$b \equiv \frac{2}{3} \tilde{\Omega} (1-e^2)^{-1/3}, \quad (133)$$

and

$$c(x) \equiv \ln x + \ln \left(2(1-e^2)^{-1/6} \right) + \frac{13}{12}. \quad (134)$$

For a given eccentricity of the halo, these curves constrain the allowed space for the BEC-CDM particle parameters $(m/m_H, g/g_H)$ for vortex formation, for which there is a minimum allowed value of $g/g_H > 1$, according to (40) (see Fig.5). This is reasonable since it makes no sense for a vortex core radius ξ to be indefinitely large. Equ.(131) also describes the critical curve $\Omega = \Omega_c$ in this parameter space¹³.

¹³ We can also solve for the critical angular velocity of the halo, Ω_c , above which a vortex is energetically favoured:

$$\begin{aligned} \Omega_c = \Omega_{QM} \left\{ \frac{3}{2} (1-e^2)^{1/3} \left[\ln \left(\frac{R}{\xi} \right) + \ln \left(2(1-e^2)^{-1/6} \right) + \frac{13}{12} \right] + \frac{3}{2} (1-e^2)^{1/3} \left(\frac{\xi}{R} \right)^2 \left(\frac{\Omega_G}{\Omega_{QM}} \right)^2 \left[(1-e^2)^{2/3} + \frac{\arcsin(e)}{e} (1-e^2)^{1/6} - \frac{\xi}{R} (1-e^2)^{1/3} \sqrt{\left(\frac{R}{\xi} \right)^2 (1-e^2)^{2/3} + 1} - \left(\frac{\xi}{R} \right)^2 \ln \left(\frac{R}{\xi} (1-e^2)^{1/3} + \sqrt{\left(\frac{R}{\xi} \right)^2 (1-e^2)^{2/3} + 1} \right) \right] - \frac{1}{8} (1-e^2)^{1/3} (A_1(e) + 5/2) \left(\frac{\Omega_G}{\Omega_{QM}} \right)^2 \left(\frac{\xi}{R} \right)^4 \right\}. \quad (135) \end{aligned}$$

This expression differs from the result given in Rindler-Daller & Shapiro (2010), since we have taken here into account the gravitational potential of the vortex more carefully. It can be shown that the general expression for

The results strongly suggest that BEC dark matter particles with smaller coupling constant, especially those without self-interaction, $g \equiv 0$, are *not* able to form a vortex.

In Fig.5 (left-hand-plot), we show the relationship (131) (i.e. m/m_H versus g/g_H) *independently* of halo size, but for given halo eccentricity, i.e. given spin parameter, $\lambda = (0.01, 0.05, 0.1)$. One can easily check on which side of the critical curves vortex formation is favoured by determining the sign of $\delta E'$. The result is that for each set of solution branches, no vortex is allowed for parameters in the space outside of the region bound by the critical curves, or with other words, only inside that bound region, for a given λ , is the vortex energy in the rotating frame negative. One can see that the parameter space of vortex existence grows as e or λ increases, as expected. However, the energy calculation did not incorporate virial equilibrium of the halo, which we have seen further constrains $(m/m_H, g/g_H)$ according to (81). We therefore also show this relationship in Fig.5 for the same e -values. The sensitivity to the eccentricities is weak, so the respective lines seem to lie on top of each other on the double-logarithmic plot. In light of the discussion in Section 2.2, we expect the virial relationship (81) to be valid only if $g/g_H \gg 2$. Now, for a given spin-parameter, virialized BEC haloes will form vortices for those $(m/m_H, g/g_H)$ -values, for which the virial line lies inside the region bound by the critical curves. The intersection of the virial line with the critical energy curve defines thus a set of critical values $(m/m_H)_{crit}, (g/g_H)_{crit}$ for each λ , above which a vortex will form. The results are shown in Table 2.

In Fig.6, we translate the bounds on vortex formation from Fig.5 to the *dimensional* BEC particle parameters m and g . To this end, a halo mass and size have to be chosen, which will fix m_H and g_H in (48) and (49), respectively. We chose a Milky-Way halo and a dwarf-galaxy-sized halo¹⁴. For the latter, the parameter space of vortex formation is shifted to higher values of particle mass as compared to the Milky-Way halo. Generally, however, the parameter space of vortex formation shifts to lower values of the particle mass for haloes of the *same* size but lower mean density.

As a further illustration of the importance of self-interaction, we plot the vortex energy $\delta E'$ of equ.(130) as a function of the spin parameter λ for several chosen values of BEC models $(m/m_H, g/g_H)$ in Fig.5, right-hand-plot. Again, we see the trend of the result in Fig.5 (lhs) at play: for a given spin-parameter λ , the vortex is increasingly favoured for larger coupling strength g/g_H . On the other hand, for fixed g/g_H , a larger spin-parameter makes the vortex favoured. So, the total energy of the system is lowered above some critical λ , which is smaller for higher values of g/g_H . For the depicted examples, we see that the BEC model of the upper curve with $(m/m_H, g/g_H) = (100, 100)$ is never able to form a vor-

equ.(135) is a monotonically increasing function of d , so our restriction to the lowest critical angular velocity for which there is $d = 1$ is well-motivated, after all. In the Thomas-Fermi regime, as $R/\xi \rightarrow \infty$, the leading-order term in the critical angular velocity diverges logarithmically, $\Omega_c \simeq \Omega_{QM} \ln(R/\xi)$, just as for laboratory condensates (see e.g. Lundh, Pethick & Smith (1997) or Pitaevskii & Stringari (2003)).

¹⁴ Note again that the critical energy curves need R and M as input, while the virial constraint needs R only to specify the dimensional (m, g) -space, see equ. (80) and (82).

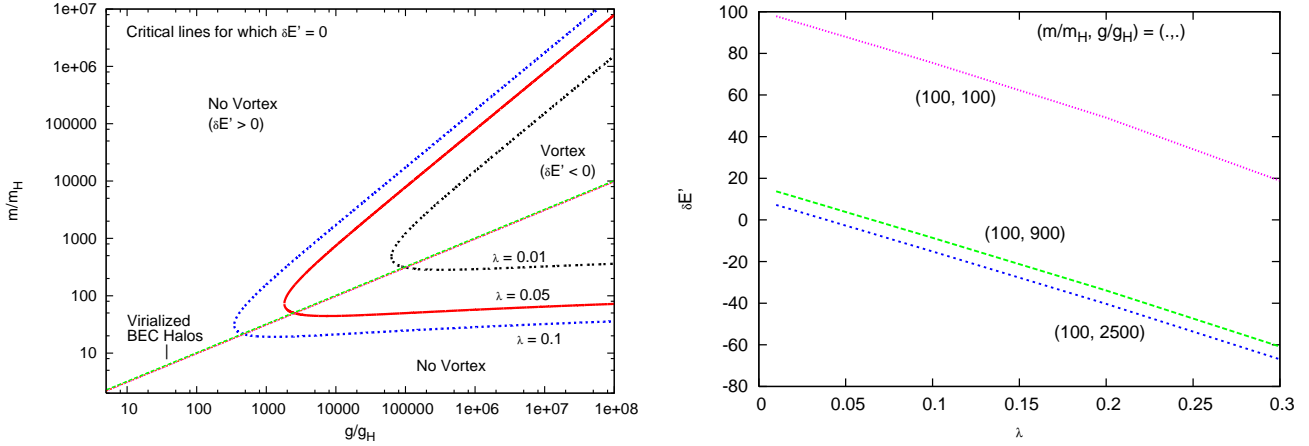


Figure 5. BEC-CDM particle parameter space and vortex energy for Halo-Model A: *Left-hand-plot:* Critical curves $\delta E' = 0$ (or $\Omega = \Omega_c$) for vortex formation in the dimensionless parameter space $(g/g_H, m/m_H)$ for $\lambda = 0.01$ ($e = 0.062$) (long-dashed black), $\lambda = 0.05$ ($e = 0.302$) (solid red), $\lambda = 0.1$ ($e = 0.550$) (short-dashed blue); BEC haloes constrained by the Virial theorem: straight lines for the same e -values. *Right-hand-plot:* Vortex energy in the rotating frame in units of $\Omega_{QM} L_{QM}$ versus λ -spin parameter for three different BEC-CDM particle models $(m/m_H, g/g_H) = (100, 100), (100, 900), (100, 2500)$.

tex, since it would cross the $(\delta E' = 0)$ -horizontal only at a λ -value, which is beyond the stability limit of the spheroidal halo, see Table A1.

We also note that the condition of a vortex to be energetically favoured, $\delta E' < 0$, does not automatically fix the numerical value of $L/L_{QM} > 1$. In fact, the value of L/L_{QM} varies along the critical energy curves in Fig.5 (lhs), being larger for higher m/m_H , according to (108). The minimum on those curves at the critical BEC-CDM particle parameters is a factor of $L/L_{QM} \simeq 4 - 6$ for the λ -values considered, see Table 2. This reflects the fact that the spheroidal haloes carry a lot of excess angular momentum over L_{QM} in all of the relevant parameter space. It seems at first sight counter-intuitive that $(L/L_{QM})_{crit}$ decreases with increasing λ . However, one must bear in mind that this result comes from critical conditions on the energy for vortex formation, i.e. if λ happens to be small, so must the ratio L/L_{QM} be large enough for a vortex to form, or, conversely, a higher λ makes a vortex possible at lower L/L_{QM} . The spin-parameter, after all, does not only depend on L , but also on the total energy E of the system, see equ.(1).

Table 2 also shows the corresponding vortex core radii for the chosen haloes, according to the relation in (41). Since the vortex core shrinks with increasing self-interaction strength (see equ.(39)), the values displayed are the maximum possible ones.

4.4 Halo-Model B: $L = L_{QM}$

4.4.1 Energy and density profiles of the irrotational Riemann-S ellipsoid

To account for the effects of compressibility and irrotationality, we take as our unperturbed halo with no vortex an $(n = 1)$ -polytropic Riemann-S ellipsoid having $L = L_{QM}$, just enough angular momentum for one quantum vortex. We will perform a similar energy analysis as in Section 4.3 to determine if a vortex, which carries all of the angular momentum, is energetically favoured. Since the vortex takes up all of the angular momentum in this model, however, the

Table 2. Halo-Model A: Lower bounds on BEC-CDM particle mass and self-interaction coupling strength for vortex formation in haloes of given spin-parameter; the corresponding ξ -values are upper bounds for the vortex core radius

Independent of halo size:			
λ	$(m/m_H)_{crit}$	$(g/g_H)_{crit}$	$(L/L_{QM})_{crit}$
0.01	309.41	$1.02 \cdot 10^5$	5.65
0.05	49.52	2549.24	4.53
0.10	21.73	454.54	4.02

Milky-Way-sized halo: $M = 10^{12} M_\odot$, $R = 100$ kpc			
λ	m_{crit} [eV]	g_{crit} [eV cm ³]	ξ_{max} [kpc]
0.01	$3.30 \cdot 10^{-23}$	$2.30 \cdot 10^{-59}$	0.31
0.05	$5.28 \cdot 10^{-24}$	$5.74 \cdot 10^{-61}$	1.98
0.10	$2.32 \cdot 10^{-24}$	$1.02 \cdot 10^{-61}$	4.69

Dwarf-galaxy-sized halo: $M = 10^{10} M_\odot$, $R = 10$ kpc			
λ	m_{crit} [eV]	g_{crit} [eV cm ³]	ξ_{max} [kpc]
0.01	$1.04 \cdot 10^{-21}$	$2.30 \cdot 10^{-58}$	0.03
0.05	$1.67 \cdot 10^{-22}$	$5.74 \cdot 10^{-60}$	0.20
0.10	$7.33 \cdot 10^{-23}$	$1.02 \cdot 10^{-60}$	0.47

final shape will be a spherical halo with a cylindrical vortex in its centre.

Before we study this in more detail, we first consider the energy of the vortex-free ellipsoidal halo model. The energy of the irrotational Riemann-S ellipsoid with $(n = 1)$ is given by (55), where we set $K_Q = 0$ and use equ.(95)-(98) for the remaining terms in order to arrive at

$$E_R = U_{SI} + W + T = \frac{\rho_c^E}{2} M \frac{g}{2m^2} - \frac{3}{4} \frac{GM^2}{R} f(e_1, e_2) + \frac{\kappa_1}{20} \mathcal{K}(e_1, e_2) M R^2 \bar{\Omega}_G^2, \quad (136)$$

where

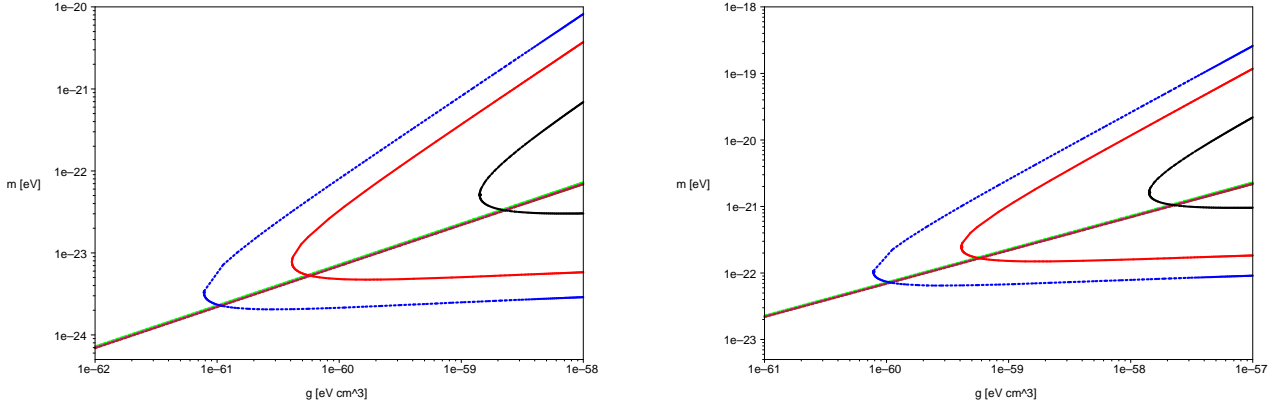


Figure 6. Critical curves $\delta E' = 0$ for vortex formation in the dimensional BEC-CDM particle parameter space for Halo-Model A: particle mass m in eV versus g in eV cm^3 for a Milky-Way-sized halo, $M = 10^{12} M_\odot$, $R = 100$ kpc (*left-hand plot*) and a dwarf-galaxy-sized halo, $M = 10^{10} M_\odot$, $R = 10$ kpc (*right-hand plot*); caption as in Fig.5 (lhs)

$$\begin{aligned}
 \mathcal{K}(e_1, e_2) &\equiv \\
 &\equiv \left((1 - e_1^2)^{-1/6} (1 - e_2^2)^{-1/6} - (1 - e_1^2)^{1/3} (1 - e_2^2)^{-1/6} \right)^2 \times \\
 &\times (\tilde{\Omega} + \tilde{\Lambda})^2 + \\
 &+ \left((1 - e_1^2)^{-1/6} (1 - e_2^2)^{-1/6} + (1 - e_1^2)^{1/3} (1 - e_2^2)^{-1/6} \right)^2 \times \\
 &\times (\tilde{\Omega} - \tilde{\Lambda})^2
 \end{aligned} \quad (137)$$

is a function of the eccentricities only. Here we defined $\tilde{\Omega}_G \equiv \sqrt{\pi G \bar{\rho}^E}$, $\tilde{\Lambda} = \Lambda / \Omega_G$ and $\bar{\rho}^E, \rho_c^E$ are the mean and central densities of the Riemann-S ellipsoid, respectively (see also *Appendix A.3*). The total angular momentum is given in (97) and we will force it to be equal to L_{QM} in the calculation of the vortex energy in the next subsection. Although we will only make use of the global energies as stated in *Section 3.2* for the calculation which follows, we find it useful to plot the actual density profiles of the Riemann-S ellipsoids in the absence of a vortex, see Fig.7 *left-hand-plot*. In fact, as we show in *Appendix A3*, analytic profiles can be derived if the ellipsoidal approximation is assumed.

4.4.2 Vortex ansatz and vortex energy

Once formed, the vortex is assumed to carry all of the angular momentum $L = L_{QM}$ of the halo. That means we anticipate a transition of the Riemann-S ellipsoid to a sphere, but with a vortex in the centre. A spherical halo with central vortex has been studied e.g. in Kain & Ling (2010), where an approximate calculation of the density profile in the presence of a vortex has been presented. For convenience, we will thus in the following take advantage of the result for the approximate energy of a spherical halo with cylindrical vortex as presented there¹⁵.

¹⁵ As we indicated in *Section 1*, the approach in Kain & Ling (2010) to calculate the energy of the halo with vortex neglects angular momentum in the first place, making the very appearance of the vortex unmotivated. However, since we start from a halo as a Riemann-S ellipsoid *with* minimum angular momentum L_{QM} , provided by the λ -spin parameter, it is meaningful to ask the question of whether it is energetically favoured to drive the system to a state having a vortex in the center.

The usual ansatz for a singly-quantized, axisymmetric vortex is used in Kain & Ling (2010), in our notation $\tilde{w} = |w|e^{i\phi}$. Then, the GP energy of a halo with such a vortex on top of the spherical background density (35) is calculated in Kain & Ling (2010). Using our notation, the energy of the spherical halo in the presence of the vortex given in equ.(6.22) of Kain & Ling (2010) is

$$\begin{aligned}
 E_S = U_{SI} + W + T = & \frac{\rho_c^S}{2} M \frac{g}{2m^2} - \frac{3}{4} \frac{GM^2}{R_0} + \\
 & + \frac{1}{4} L_{QM} \Omega_{QM} (1 + \pi Si(\pi) (\ln 2 + \ln(R_0/R_c)) + \pi \Gamma), \quad (138)
 \end{aligned}$$

where $Si(\pi) \approx 1.852$ is the sine integral evaluated at π , $\Gamma \approx -2.658$, and ρ_c^S is the central density of the halo, which is an $(n = 1)$ -polytropic *sphere* with radius R_0 given in (37). Some shortcomings enter their calculation of the angular kinetic part of the vortex energy: the actual vortex profile, as for instance given by $|w|^2$ in equ.(119), is replaced by a finitely thick, empty cylinder with radius R_c , in our notation $R_c = \xi \sqrt{\bar{\rho}^E / \rho_c^S}$. Also, the change in the gravitational potential due to the vortex is neglected as can be seen in the derivation of equ.(6.22) in Kain & Ling (2010)¹⁶. Using their result for the energy of the spherical halo in the presence of the vortex provides us thus with a rougher upper bound estimate of the conditions for vortex formation, than if we had used a better implementation of the vortex ansatz of *Section 4.3.1* in the Riemann-S ellipsoid. However, given the orders of magnitudes involved in the resulting bounds on the BEC particle parameters, we do not expect these effects to be very significant. We stress that the above expression for the energy, equ. (138), assumes that all of the angular momentum is in the singly-quantized vortex, whose amount is $L_{QM} = N\hbar$. Equ.(138) is the energy as measured in the *rest frame*, therefore $E'_S = E_S - \Omega L_{QM}$ is the energy in the frame rotating rigidly with Ω . The energy in (136) is also the one given in the rest frame, so again $E'_R = E_R - \Omega L$ is the energy in the rotating frame. Now, in order to compare the two states on an equal footing, we force the Riemann-S

¹⁶ More precisely, the gravitational potentials V_G in equ.(6.8) and (6.13) of Kain & Ling (2010) are simply set equal, whereas our analysis in *Section 4.3.1* clearly distinguishes between the unperturbed halo potential Φ_0 and the perturbed one, Φ .

ellipsoid to have the same amount of angular momentum as the sphere with vortex, i.e. all of the angular momentum of the ellipsoid shall be transferred to the vortex, leaving the bulk of the halo spherical. We will thus set $L = L_{QM}$ in E'_R . Moreover, since the total mass M of the halo shall not change across the transition to the vortex state, the mean and central densities, $\bar{\rho}^S, \bar{\rho}^E$ and ρ_c^S, ρ_c^E , for the spherical and the ellipsoidal halo shape, respectively, will differ but be related according to

$$\bar{\rho}^E = \bar{\rho}^S g(e_1, e_2)^{3/2} \text{ and } \rho_c^E = \rho_c^S g(e_1, e_2)^{3/2}, \quad (139)$$

where we used $\bar{\rho}^E = 3M/(4\pi R^3)$ and (101) (see also equ.(3.10) in LRS93). Furthermore, by using (139) and (36), we can write $\bar{\rho}^E/\rho_c^E = \frac{3}{\pi^2} g(e_1, e_2)^{3/2}$, which we use in (138) in order to rewrite

$$\ln(R_0/R_c) = \ln R/\xi + \frac{1}{2} \ln(\pi^2/3g(e_1, e_2)^{1/2}). \quad (140)$$

Calculating the energy difference and rearranging terms, we get for the (dimensionless) vortex energy,

$$\begin{aligned} \frac{\delta E'}{\Omega_{QM} L_{QM}} &\equiv \frac{E'_S - E'_R}{\Omega_{QM} L_{QM}} = \frac{E_S - E_R}{\Omega_{QM} L_{QM}} = \\ &= \frac{\pi^2}{24} (f(e_1, e_2)^{-3/2} - 1) \left(\frac{g}{g_H} \right) + \frac{\pi Si(\pi)}{8} f(e_1, e_2)^{-1} \ln \frac{g}{g_H} - \\ &- \left[g(e_1, e_2)^{-1/2} - f(e_1, e_2) \right] \left(\frac{m}{m_H} \right)^2 + \frac{1}{4} g(e_1, e_2)^{-1} \times \\ &\times \left[1 + \pi Si(\pi) \ln 2 + \pi \Gamma + \frac{\pi Si(\pi)}{2} \ln \left(\frac{\pi^2}{3g(e_1, e_2)^{1/2}} \right) - \right. \\ &\left. - \frac{\kappa_1}{5} \mathcal{K}(e_1, e_2) g(e_1, e_2) \left(\frac{m}{m_H} \right)^2 \right]. \end{aligned} \quad (141)$$

We stress again that formula (141) has been derived by imposing $L = L_{QM}$. In Fig.7, *right-hand-plot*, we show a spherical halo with central vortex which transitioned from a Riemann-S ellipsoid having $\lambda = 0.05$.

In Fig.8, left-hand-plot, we show virialized haloes which are irrotational Riemann-S ellipsoids according to (103) for $\lambda = (0.01, 0.05, 0.1)$: Thanks to the relationship in (109), the constraint of having minimum angular momentum for vortex formation, $L = L_{QM}$, means to fix the value of m/m_H . For given λ and m/m_H , the Virial constraint (103) fixes then the self-interaction g/g_H . This means that the condition $L = L_{QM}$ can be met at only *one* point (for each λ) in the BEC-CDM particle parameter space. These points are also depicted in Fig.8. Inserting those values for the particle parameters in (141) shows that the corresponding vortex energy is negative, i.e. the vortex is favoured for all λ -values of interest. Again, the vortex is favoured at high enough particle mass and self-interaction strength for a given λ . To strengthen this picture by adding more 'data points', we plot (103) for a larger range in λ according to Table A2 and the corresponding values $(m/m_H, g/g_H)$ at which $L = L_{QM}$ (see Fig.8, right-hand-plot). A vortex can be formed in all cases considered. In addition, Fig.9 confirms the previous result of favouring vortices at high enough self-interaction for a given λ and vice versa. Since vortex formation generally requires $L \geq L_{QM}$, the above calculation provides us thus again with the *critical* BEC-CDM particle parameters, above which vortex formation is favoured, along with

Table 3. *Halo-Model B*: Lower bounds on BEC-CDM particle mass and self-interaction coupling strength for vortex formation in haloes of given spin-parameter; the corresponding ξ -values are upper bounds for the vortex core radius

Independent of halo size:			
λ	$(m/m_H)_{crit}$	$(g/g_H)_{crit}$	L/L_{QM}
0.01	44.58	1595.07	1
0.05	9.49	68.00	1
0.10	5.01	17.20	1

Milky-Way-sized halo: $M = 10^{12} M_\odot$, $R = 100$ kpc			
λ	m_{crit} [eV]	g_{crit} [eV cm ³]	ξ_{max} [kpc]
0.01	$4.75 \cdot 10^{-24}$	$3.59 \cdot 10^{-61}$	2.50
0.05	$1.01 \cdot 10^{-24}$	$1.53 \cdot 10^{-62}$	12.13
0.10	$5.34 \cdot 10^{-25}$	$3.87 \cdot 10^{-63}$	24.11

Dwarf-galaxy-sized halo: $M = 10^{10} M_\odot$, $R = 10$ kpc			
λ	m_{crit} [eV]	g_{crit} [eV cm ³]	ξ_{max} [kpc]
0.01	$1.50 \cdot 10^{-22}$	$3.59 \cdot 10^{-60}$	0.25
0.05	$3.20 \cdot 10^{-23}$	$1.53 \cdot 10^{-61}$	1.21
0.10	$1.69 \cdot 10^{-23}$	$3.87 \cdot 10^{-62}$	2.41

the maximum vortex core sizes. Table 3 summarizes those parameters in dimensionless and physical units. Owing to the constraint $L = L_{QM}$, we do not calculate the critical condition $\delta E' = 0$ in *Halo-Model B*, since that condition is fulfilled at another L ($\neq L_{QM}$). Apart from the consideration, that this model may be more realistic than the rigidly rotating haloes of *Model A* in *Section 4.3*, the purpose of this model was also to show that the results gained in *Section 4.3* are consistent with those derived here, despite the simplifying assumptions on the unperturbed (vortex-free) halo, on which the former were based. The same trend can be seen here as in *Model A* of *Section 4.3*: vortex formation requires a high enough mass m and positive self-interaction g of the BEC-CDM particles, where smaller λ -spin parameters require higher values for m and g . Small-mass haloes set tighter constraints on the particle parameters. Both halo models are thus qualitatively consistent with each other. For the same halo with fixed λ , *Model A*, however, requires in general larger values of m and g than *Model B*. This is due to the fact, that *Model A* has more angular momentum $L/L_{QM} \gg 1$, resulting in higher m/m_H via (108), which in turn requires higher g/g_H due to the virial constraint (81). By the same token, the maximum vortex core radii can be substantially larger in *Halo-Model B*, since the critical self-interaction strengths for vortex formation are smaller than for *Halo-Model A*.

We also see from Fig.8 that a significant portion of the particle parameter space remains, where vortices will not form. In fact, for all values of $(g/g_H, m/m_H)$ which lie left to the depicted points on a given virial curve, depending on λ , haloes fulfill $L < L_{QM}$. For coupling strengths which are high enough for them to be still in the polytropic Thomas-Fermi regime, $g/g_H \gg 2$, those haloes will just remain compressible, irrotational Riemann-S ellipsoids, and will not undergo vortex formation.

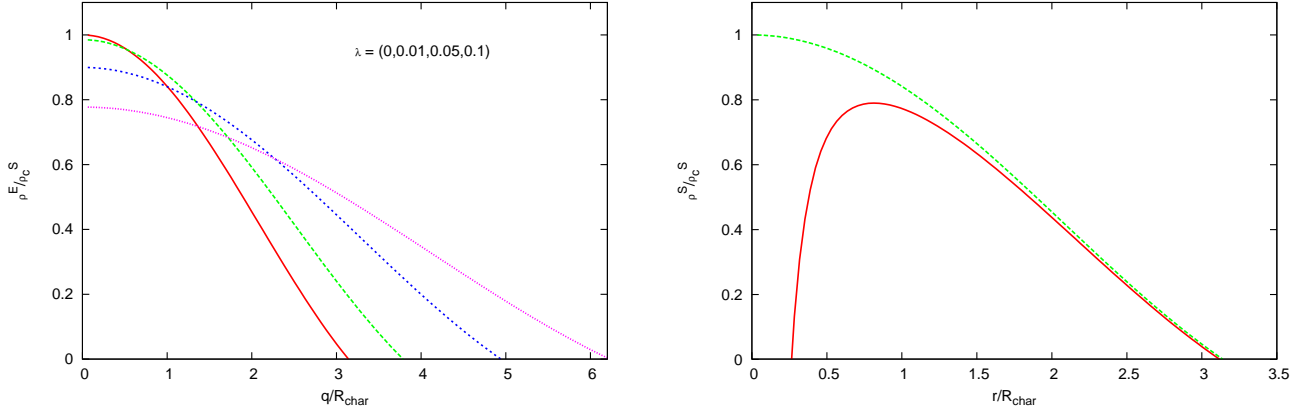


Figure 7. Density profiles for Halo-Model B: *Left-hand-plot*: Profiles of the (vortex-free) ($n = 1$)-polytropic Riemann-S ellipsoidal haloes having $\lambda = (0.01, 0.05, 0.1)$, employing the ellipsoidal approximation, according to equ.(A22). The solid curve is the ($n = 1$)-polytropic sphere, equ.(35), and is added for comparison. The densities are all normalized to $\rho_c^S = 1$. The locus of the outer surface where the density vanishes increases with λ ; *Right-hand-plot*: Profile of the spherical halo with vortex in the centre (solid) using equ.(4.16) of Kain & Ling (2010) with $\Theta_0 = 1$ and R_c/ξ for $\lambda = 0.05$. The unperturbed sphere (dashed) is added for comparison.

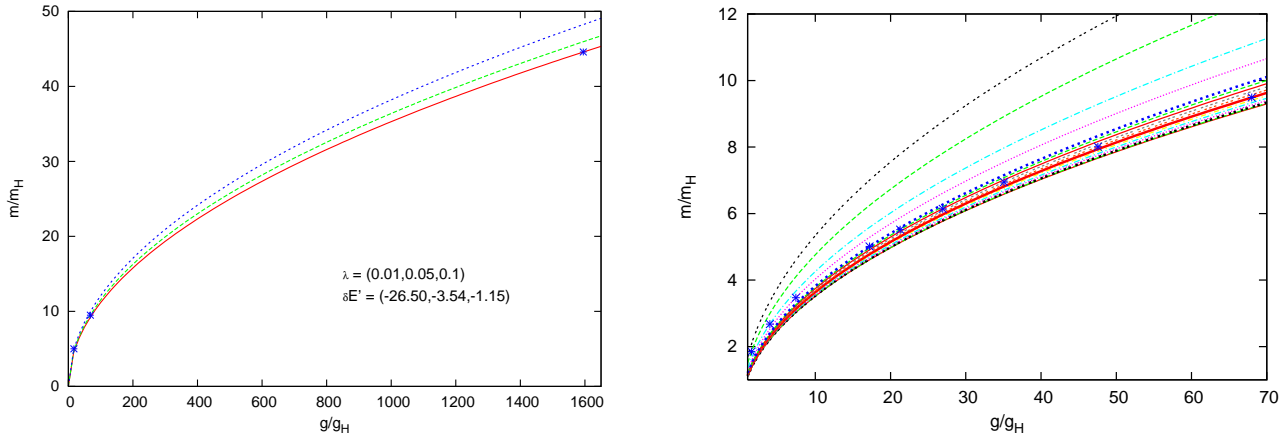


Figure 8. BEC-CDM particle space for Halo-Model B (no logarithmic scales here !): *Left-hand-plot*: Virialized haloes according to (103) for $\lambda = (0.01, 0.05, 0.1)$ (lower to upper curves) with depicted points $(m/m_H, g/g_H)$, according to Table 3, at which $L = L_{QM}$ and corresponding vortex energy $\delta E'$; *Right-hand-plot*: the same but including more curves in λ according to Table A2, and zoomed-in closer to the origin; dots denote BEC haloes having $L = L_{QM}$.

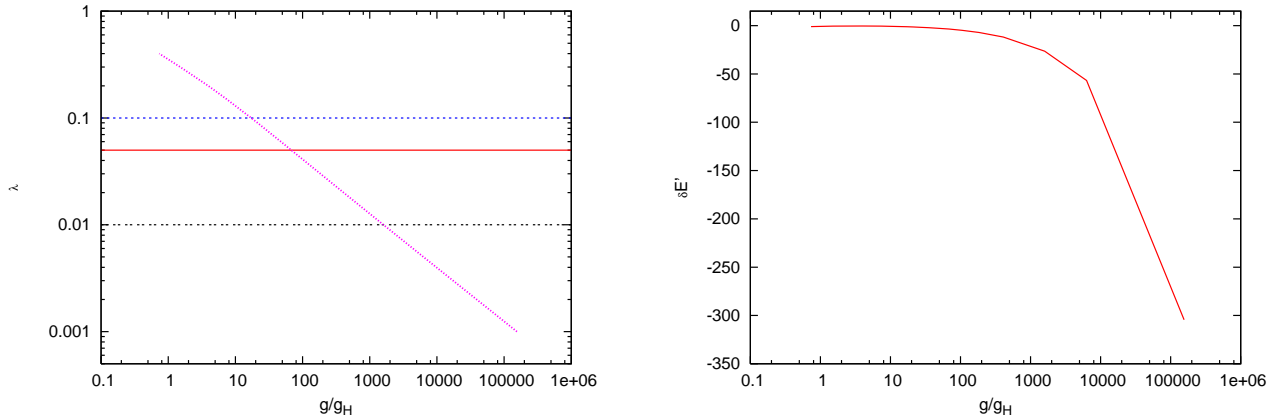


Figure 9. Halo-Model B: Virialized BEC haloes according to (103) for which $L = L_{QM}$: *Left-hand plot*: spin parameter vs. self-interaction coupling strength; *Right-hand-plot*: Vortex energy (141) in units of $\Omega_{QM} L_{QM}$ vs. self-interaction strength.

5 CONCLUSIONS AND DISCUSSION

We have studied in this paper the conditions of vortex formation in galactic haloes composed of dark matter particles which are able to form a Bose-Einstein condensate. Haloes can then be described as fluids, obeying quantum-mechanical fluid equations. Quantum-mechanical effects make this form of dark matter behave differently from standard CDM, resulting in new effects with potentially observable consequences. There are essentially two limiting cases one may consider. First, for quantum-coherence to be relevant on the scale of a halo of radius R , we must either require the particle de-Broglie wavelength (21) to be of the order of the halo size, $\lambda_{dB} \lesssim R$, or else require $\lambda_{dB} \ll R$ but with a strong enough repulsive self-interaction to hold the halo up against gravity. In the former case, if $v \simeq v_{vir}$ for the halo, this translates into a condition for the dark matter particle mass to be small enough, $m \gtrsim m_H = 1.066 \cdot 10^{-25} (R/100 \text{ kpc})^{-1/2} (M/10^{12} M_\odot)^{-1/2}$ eV. In the latter case, in order for the repulsive self-interaction pressure force greatly to exceed that due to quantum pressure (i.e. the Thomas-Fermi regime), we must require $g \gg g_H = 2.252 \cdot 10^{-64} (R/100 \text{ kpc}) (M/10^{12} M_\odot)^{-1}$ eV cm³. BEC haloes can then be approximated by polytropes with index $n = 1$. If we take R to be the radius of the virialized object supported against gravity by the dominant, repulsive self-interaction, this condition becomes a condition on the particle mass given by $m \gtrsim \frac{m_H}{4} \sqrt{15g/g_H}$.

These results apply generally to the global halo structure. However, rotating BEC haloes add new phenomenology, and the possibility to distinguish this form of dark matter from other candidates. To this aim, we have studied here the question of whether an angular velocity sufficient to create vortices occurs in BEC-CDM cosmologies. As quantum fluid systems, BEC haloes can be modelled as uniformly rotating ellipsoids, with and without internal motions superposed. To this aim, we have derived equations which relate the eccentricities of haloes to their λ -spin parameter. Once the latter is fixed, the eccentricities can be uniquely determined. Then, we have analytically studied necessary and sufficient conditions for vortex formation. Vortex formation requires as a necessary minimum condition that the halo angular momentum fulfills $L \geq L_{QM} = N\hbar$, which implies a lower bound on m/m_H , i.e. on the dark matter particle mass. However, a sufficient condition for vortex formation can be established by an energy analysis, which aims to find the conditions when a vortex becomes energetically favoured. This results, in addition, to lower bounds on the positive self-interaction coupling strength of the dark matter particle, g/g_H . While the sufficient condition also requires $L \geq L_{QM}$, the amount necessary is determined by the model.

We have studied two classes of models for rotating haloes in order to analyze stability with respect to vortex formation in two limits, that for $L/L_{QM} \gg 1$ (*Halo-Model A*) and for $L/L_{QM} = 1$ (*Halo-Model B*), respectively. In *Halo-Model A*, haloes are modelled as homogeneous Maclaurin spheroids. The minimum angular momenta for vortex formation are then $(L/L_{QM})_{crit} = (5.65, 4.53, 4.02)$ for $\lambda = (0.01, 0.05, 0.1)$, respectively, which correspond to a constraint on the particle mass $m/m_H \geq (m/m_H)_{crit}$, where $(m/m_H)_{crit} = (309.41, 49.52, 21.73)$, respectively. As long

as m/m_H satisfies this condition, the strength of the self-interaction must also then satisfy the condition that $g/g_H \geq (g/g_H)_{crit}$, where $(g/g_H)_{crit} = (1.02 \cdot 10^5, 2549.24, 454.54)$ for these same λ -values, respectively.

However, for *Halo-Model B*, which is an ($n = 1$)-polytropic Riemann-S ellipsoid, strictly irrotational prior to vortex formation, even $L/L_{QM} = 1$ can be sufficient for vortex formation, if the self-interaction strength is large enough. The condition $L/L_{QM} = 1$ fixes the value of m/m_H for each λ according to (109), and the condition of Virial equilibrium (103) thereby also fixes g/g_H . For $\lambda = (0.01, 0.05, 0.1)$, these values are given by $m/m_H = (44.58, 9.49, 5.01)$ and $g/g_H = (1595.07, 68.00, 17.20)$, respectively. According to equ.(141), *Halo-Model B* makes vortex formation energetically favourable for those values of m/m_H and g/g_H . We interpret this to mean that, for $L/L_{QM} > 1$ (i.e. $m/m_H > (m/m_H)(L = L_{QM})$), vortex formation will *also* be favoured, as long as $g/g_H > (g/g_H)(L = L_{QM})$. Furthermore, any values of m/m_H and g/g_H which satisfy the condition for vortex formation in *Halo-Model A* will automatically satisfy that found by *Halo-Model B*, which is less stringent, although more accurate.

We can thus imagine vortex formation in BEC haloes composed of repulsively interacting particles as follows: If the angular momentum of a rotating BEC halo fulfills $L < L_{QM}$ (i.e. if $(m/m_H) < (m/m_H)_{crit}$ for a given λ , according to *Halo-Model B*), no vortex will form, and the halo can be modelled by a mildly compressible, irrotational Riemann-S ellipsoid, which has a polytropic index of $n = 1$. For $L = L_{QM}$ (i.e. if $m/m_H = (m/m_H)_{crit}$), the irrotational Riemann-S ellipsoidal halo can make a transition to a non-rotating, spherical halo with a vortex at the center if the self-interaction is strong enough (i.e. $g/g_H = (g/g_H)_{crit}$). For a range of angular momenta fulfilling $L_{QM} < L \leq 2L_{QM}$, we may still expect a central vortex but now with the excess angular momentum deforming the halo such that again a Riemann-S ellipsoid forms. Finally, if $L \gg L_{QM}$, oblate haloes described as Maclaurin spheroids can have a central vortex if $m/m_H \geq (m/m_H)_{crit}$ and $g/g_H \geq (g/g_H)_{crit}$ with the critical values now given by *Halo-Model A*. Those critical values determine as of when a single vortex is energetically favoured, but since $L/L_{QM} \gg 1$ [i.e. (L per particle) $\gg \hbar$], it is also possible that multiple vortices will form, even a lattice of vortices¹⁷. For a dense lattice of vortices, the halo's vorticity will approach that of a rigidly rotating body, according to the quantum-mechanical correspondence principle argument, applied to the analogous problem in superfluid helium by Feynman (1955). A suitable generalization of the homogeneous *Halo-Model A* of Section 3.1 to compressible spheroidal haloes, according to the ellipsoidal approximation of Lai, Rasio & Shapiro (1993), will then constitute a viable model for this high-angular momentum regime.

Generally, we have shown that BEC-CDM haloes in the polytropic Thomas-Fermi regime *will* typically form vortices, since this regime requires $m \gg m_H$ and $g \gg g_H$, which largely overlaps the region of parameter space for

¹⁷ It is known that laboratory BEC quantum gases confined by a wide range of trap potentials favour multiple vortices that are singly-quantized over a single vortex that is multiply-quantized, see e.g. Aftalion & Du (2001); Rindler-Daller (2008).

vortex formation. By comparing the characteristic parameters of *Section 2.3* with the constraints derived for vortex formation, we see that, apparently, for these values of particle parameters, the angular momentum of CDM haloes is typically of the order of the minimum value required for quantum vortex formation. Since vortex formation happens then in a large part of the particle parameter space, this is important to take into account when BEC-CDM models are fitted to galactic rotation curves and density profiles, especially in the very centers. While it is true that the vortex becomes more and more favoured for increasing self-interaction strengths g/g_H , its size, and hence its dynamical importance, *decreases*. However, at the critical values for vortex formation and beyond, the size of the vortex in both halo models is large enough to be expected to be able to imprint a notable effect on the central halo dynamics, which can be seen from Tables 2 and 3.

The appearance of vortices in the central parts of BEC-CDM haloes, whose core regions are depleted of dark matter mass, will change the gravitational coupling to baryons, as compared to a smooth or nearly-smooth dark matter distribution in the halo. As a result of depleted dark matter in the vortex cores, the subsequent collapse of baryonic matter can be delayed and so can star formation. A detailed analysis is necessary, however, to be able to quantify those effects.

Our results show furthermore that haloes with particles of high enough mass to satisfy the minimum condition that $L \geq L_{QM}$ are nevertheless vortex-free, *unless* their self-interaction strength is high enough. In particular, vortices will not form in BEC dark matter which has no self-interaction, $g = 0$. Axions have often been modelled without self-interaction, but in doing so they will not be able to form vortices in galactic haloes, contrary to what has been proposed in Sikivie & Yang (2009). In order to have vortices mimic a net rotational component, a dense lattice of vortices is needed. Both halo models studied here are in principle able to sustain these structures. However, not only is it required that $L \gg L_{QM}$, but so is positive self-interaction. On the other hand, our analysis does not simply extend to cases when $g < 0$, such that the small attractive interaction of axions can be taken into account. While we do still not expect quantum vortices to appear in this case, other defect structures, like bright solitons, have been shown to being able to form not only in laboratory BECs with attractive self-interaction, but also in some models of axion haloes, see Mielke & Vélaz Pérez (2007, 2009).

Our results also indicate that there remain notable regions in (m, g) -parameter space where vortices are *not* favoured. In these cases, rotating haloes may be modelled as irrotational, compressible ($n = 1$)-polytropic Riemann-S ellipsoids, as we have shown.

We have considered here the case of BEC-CDM which is a pure, i.e. zero-temperature, condensate. In the Thomas-Fermi regime, the characteristic size of virialized objects is in that case the radius of an $(n = 1)$ -polytrope, fixed by the ratio g/m^2 of particle parameters. As mentioned in *Section 2.2*, this can be interpreted either as the full size of a halo or as the size of the core region of a larger halo. Recently, Slepian & Goodman (2011) have replaced the assumption of zero-temperature condensate by that of thermodynamic equilibrium in isothermal haloes at the virial temperature. The haloes which result contain an $(n = 1)$ -polytropic

core of condensate surrounded by an 'atmosphere' of non-condensed bosons. They claim that such haloes are incompatible with astronomical constraints. However, as they point out, their assumption of thermodynamic equilibrium at finite temperature breaks down if the 2-body elastic scattering collision time exceeds a Hubble time, depending upon the ratio σ_s/m with the scattering cross section in equ.(6). In order to guarantee local thermodynamic equilibrium, they must assume $\sigma_s/m \approx 1 \text{ cm}^2/\text{g}$. In fact, this condition is *not* met by the ultra-light bosons considered here, for which σ_s/m is much smaller. Using equ.(6) and (7), along with (37) and (48), we can write

$$\frac{\sigma_s}{m} = 2.094 \cdot 10^{-102} \left(\frac{m}{m_H} \right)^5 \times \left(\frac{R}{100 \text{ kpc}} \right)^{3/2} \left(\frac{M}{10^{12} M_\odot} \right)^{-5/2} \frac{\text{cm}^2}{\text{g}}, \quad (142)$$

which is valid as long as $m/m_H \gg 1$. Even for large m/m_H , and for that matter, also for the critical values for the dark matter particle mass for vortex formation calculated above, the value of σ_s/m is much, much smaller than $1 \text{ cm}^2/\text{g}$.

Acknowledgements

We thank Pierre Sikivie, and Steven Weinberg, Ei-ichiro Komatsu and other members of the Texas Cosmology Center for stimulating discussion. We are especially grateful to Stuart Shapiro for his helpful comments on the effects of compressibility on rotating figures of equilibrium. This work was supported in part by U.S. NSF grants AST-0708176 and AST-1009799, NASA grants NNX07AH09G, NNG04G177G, NNX11AE09G, and Chandra grant SAO TM8-9009X to PRS. TRD also acknowledges support by the Texas Cosmology Center of the University of Texas at Austin and by the German DFG through FG960.

REFERENCES

- Aftalion A., Du Q., 2001, Phys.Rev.A, 64, 063603
- Ahn K., Shapiro P.R., 2005, MNRAS, 363, 1092
- Alcubierre M., Guzmán F.S., Matos T., Núñez D., Ureña-López L.A., Wiederhold P., 2002, Class.Quant.Grav., 19, 5017
- Antonucci-Delogu V., Dobrotka A., Becciani U., Cielo S., Giocoli C., Macciò A.V., Romeo-Veloná A., 2010, MNRAS, 407, 1338
- Arbey A., Lesgourgues J., Salati P., 2003, Phys.Rev.D, 68, 023511
- Arkani-Hamed N., Dimopoulos S., Dvali G., 1999, Phys.Rev.D, 59, 086004
- Arvanitaki A., Dimopoulos S., Dubovsky S., Kaloper N., March-Russell J., 2010, Phys.Rev.D, 81, 123530
- Asztalos S.J. et al., 2010, Phys.Rev.Lett., 104, 041301
- Baldeschi M.R., Gelmini G.B., Ruffini R., 1983, Phys.Lett.B, 122, 221
- Barnes J., Efstathiou G., 1987, ApJ, 319, 575
- Binney J., Tremaine S., 1987, Galactic Dynamics, Princeton Series in Astrophysics, Princ.Univ.Press, Princeton, NJ

- Böhmer C.G., Harko T., 2007, JCAP, 06, 025
- Böhmer C.G., Martins C.F., Salucci P., private communication (2009)
- Carroll S.M., 1998, Phys.Rev.Lett., 81, 3067
- Chandrasekhar S., 1939, Stellar Structure, Univ.Chicago Press, Chicago
- Chandrasekhar S., 1969, Ellipsoidal Figures of Equilibrium, Yale Univ.Press, New Haven
- Chavanis P.H., 2011, Phys.Rev.D, 84, 043531
- Chavanis P.H., 2012, A&A, 537, A127
- Chou A.S. et al., 2008, Phys.Rev.Lett., 100, 080402
- Colpi M., Shapiro S.L., Wasserman I., 1986, Phys.Rev.Lett., 57, 2485
- Duffy L.D., Sikivie P., 2008, Phys.Rev.D, 78, 063508
- Fetter A.L., 1974, J.Low Temp.Phys., 16, 533
- Feynman R.P., 1955, Prog.Low Temp.Phys., 1, 17
- Fukuyama T., Morikawa M., Tatekawa T., 2008, JCAP, 06, 033
- Goodman J., 2000, New Astronomy, 5, no.2, 103
- Gottlöber S., Yepes G., 2007, ApJ, 664, 117
- Graham P.W., Rajendran S., 2011, Phys.Rev.D, 84, 055013
- Guzmán F.S., Ureña-López L.A., 2004, Phys.Rev.D, 69, 124033
- Günther U., Zhuk A., 1997, Phys.Rev.D, 56, 6391
- Harko T., 2011, MNRAS, 413, 4, 3095
- Hernandez X., Park C., Cervantes-Sodi B., Choi Y.-Y., 2007, MNRAS, 375, 163
- Horava P., Witten E., 1996, Nucl.Phys.B, 460, 506
- Hu W., Barkana R., Gruzinov A., 2000, Phys.Rev.Lett., 85, 1158
- Ipsier J., Sikivie P., 1983, Phys.Rev.Lett., 50, 925
- Jäckel J., Ringwald A., 2010, Ann.Rev.Nucl.Part.Sci., 60, 405
- Kain B., Ling Y., 2010, Phys.Rev.D, 82, 064042
- Kaup D.J., 1968, Phys.Rev., 172, 1331
- Khlopov M.Y., Malomed B.A., Zeldovich Y.B., 1985, MNRAS, 215, 575
- Koda J., Shapiro P.R., 2011, MNRAS, 415, 1125
- Lai D., Rasio F.A., Shapiro S.L., 1993, ApJ Suppl., 88, 205; LRS93
- Lee J.W., Koh I.G., 1996, Phys.Rev.D, 53, 2236
- Lee J.-W., Lim S., 2010, JCAP, 7, 01
- Lundh E., Pethick C.J., Smith H., 1997, Phys.Rev.A, 55, 2126
- Lundgren A.P., Bondarescu M., Bondarescu R., Balakrishna J., 2010, ApJL, 715, L35
- Madison K.W., Chevy F., Wohlleben W., Dalibard J., 2000, Mod.Opt., 47, 2715
- Marsh D.J.E., Ferreira P.G., 2010, Phys.Rev.D, 82, 103528
- Matos T., Ureña-López L.A., 2001, Phys.Rev.D, 63, 063506
- Membrado M., Pacheco A.F., Sañudo J., 1989, Phys.Rev.A, 39, 4207
- Mielke E.W., Vélez Pérez J.A., 2007, Phys.Rev.D, 75, 043504
- Mielke E.W., Vélez Pérez J.A., 2009, Phys.Lett.B, 671, 174
- O'Dell D., Giovanazzi S., Kurizki G., Akulin V.M., 2000, Phys.Rev.Lett., 84, 5687
- Peebles P.J.E., 2000, ApJ, 534, 2, L127
- Pitaevskii L.P., Stringari S., 2003, Bose-Einstein Condensation, The Int.Ser.of Monogr.Phys. Vol.116, Eds: Birman J., Edwards S.F., Friend R., Llewellyn-Smith C.H., Rees M., Sherrington D., Veneziano G., Oxford Science Publ., Clarendon Press, Oxford
- Plionis M., Basilakos S., Ragone-Figueroa C., 2006, ApJ, 650, 770
- Porciani C., Dekel A., Hoffman Y., 2002, MNRAS, 332, 325
- Porciani C., Dekel A., Hoffman Y., 2002, MNRAS, 332, 339
- Press W.H., Ryden B.S., Spergel D.N., 1990, Phys.Rev.Lett., 64, 1084
- Recati A., Zambelli F., Stringari S., 2001, Phys.Rev.Lett., 86, 377
- Rindler-Daller T., 2008, Physica A, 387, 1851
- Rindler-Daller T., Shapiro P.R., 2010, ASP Conf.Ser. Vol.432, p.244, New Horizons in Astronomy: Frank N. Bash Symposium 2009, Eds: Stanford L.M., Green J.D. Hai L., Mao Y., Astron. Soc.Pac., San Francisco
- Ruffini R., Bonazzola S., 1969, Phys.Rev., 187, 1767
- Ryan F.D., 1997, Phys.Rev.D, 55, 6081
- Schunck F.E., 1998, ASP Con.Ser. Vol.136, p.403, Ed: Zaritsky D., Astron.Soc.Pac., San Francisco
- Schunck F.E., Fuchs B., Mielke E.W., 2006, MNRAS, 369, 485
- Short C.J., Coles P., 2006, JCAP, 12, 012
- Sikivie P., 1983, Phys.Rev.Lett., 51, 1415
- Sikivie P., Yang Q., 2009, Phys.Rev.Lett., 103, 111301
- Silverman M.P., Mallet R.L., 2002, Gen.Rel.Grav., 34, 633
- Sin S.J., 1994, Phys.Rev.D, 50, 3650
- Slepian Z., Goodman J., arXiv:1109.3844v1
- Spergel D.N., Steinhardt P.J., 2000, Phys.Rev.Lett., 84, 3760
- Ureña-López L.A., 2009, JCAP, 01, 014
- Ureña-López L.A., Guzmán F.S., 2003, Phys.Rev.D, 68, 024023
- Widrow L.M., Kaiser N., 1993, ApJ, 416, L71
- Woo T.-P., Chiueh T., 2009, ApJ, 697, 850
- Yoshida S., Eriguchi Y., 1997, Phys.Rev.D, 56, 762
- Yu R.P., Morgan M.J., 2002, Class.Quant.Grav., 19, L157

APPENDIX A: APPROXIMATE EQUILIBRIUM ROTATING FIGURES AS HALO MODELS

A1 General relationships

In this appendix, we summarize some of the properties of the homogeneous Maclaurin spheroid and irrotational, ($n = 1$)-polytropic Riemann-S ellipsoid used in this paper. A thorough treatment of these figures of rotation can be found in the works of Chandrasekhar (1969) and Lai, Rasio & Shapiro (1993) (LRS93). We make use of uniformly rotating figures as models for haloes with non-vanishing angular momentum. We assume haloes to rotate about their z -axis with angular velocity $\Omega = (0, 0, \Omega)$. Their mass density is $\rho_0 = m|f|^2$ with f the corresponding (vortex-free) halo BEC wavefunction and their semi-axes (a_1, a_2, a_3) are along (x, y, z) . The mean radius of the ellipsoids is defined as $R = (a_1 a_2 a_3)^{1/3}$, which differs from the equilibrium radius R_0 of the spherical polytrope according to equ.(77)-(78) (or (A6)) for the Maclaurin spheroid, and equ.(101) & (37) (or (A13)) for the irrotational Riemann-S ellipsoid, respectively.

The gravitational potential inside a homogeneous ellipsoidal body is given by

$$\Phi_0(x, y, z) = \pi G \rho_0 (A_1 x^2 + A_2 y^2 + A_3 z^2 - A_1 a_1^2 - A_2 a_2^2 - A_3 a_3^2) \quad (\text{A1})$$

(see e.g. Chandrasekhar (1969)), where the functions A_1, A_2, A_3 , depending on the axis ratios $a_2/a_1, a_3/a_1$ or eccentricities

$$e_1 = \sqrt{1 - (a_2/a_1)^2}, \quad e_2 = \sqrt{1 - (a_3/a_1)^2},$$

respectively, are given by

$$A_1 = 2 \frac{a_2}{a_1} \frac{a_3}{a_1} \frac{F(\theta, \phi) - E(\theta, \phi)}{\sin^3 \phi \sin^2 \theta}, \quad (\text{A2})$$

$$A_2 = 2 \frac{a_2}{a_1} \frac{a_3}{a_1} \frac{E(\theta, \phi) - F(\theta, \phi) \cos^2 \theta - \frac{a_3}{a_2} \sin^2 \theta \sin \phi}{\sin^3 \phi \sin^2 \theta \cos^2 \theta}, \quad (\text{A3})$$

$$A_3 = 2 \frac{a_2}{a_1} \frac{a_3}{a_1} \frac{\frac{a_2}{a_3} \sin \phi - E(\theta, \phi)}{\sin^3 \phi \cos^2 \theta} \quad (\text{A4})$$

with $\cos \phi = a_3/a_1$, $\sin \theta = \sqrt{\frac{1 - (a_2/a_1)^2}{1 - (a_3/a_1)^2}}$ and the standard incomplete elliptic integrals

$$E(\theta, \phi) = \int_0^\phi (1 - \sin^2 \theta \sin^2 \phi')^{1/2} d\phi',$$

$$F(\theta, \phi) = \int_0^\phi (1 - \sin^2 \theta \sin^2 \phi')^{-1/2} d\phi'.$$

The functions A_1, A_2, A_3 are generally defined this way, however, equ.(A1) is only valid for homogeneous bodies. While we use Φ_0 for the homogeneous Maclaurin spheroid explicitly in the calculations for *Halo-Model A*, we do not need to use the gravitational potential of the compressible Riemann-S ellipsoid for *Halo-Model B*, since we make use of the global energy quantities, like for instance W , as provided by LRS93.

A2 Homogeneous Maclaurin spheroids

For the Maclaurin spheroid of *Section 3.1*, $a_1 = a_2 \equiv a$, $a_3 \equiv c$ and (A1) reduces to (62). Most of the needed relationships can be already found in the main text. Similarly to LRS93, we can write the dimensionless forms of W (66) and R (77) as well as L (68) as functions of the eccentricity only:

$$|\tilde{W}| \equiv \frac{5}{3} \frac{|W|}{(GM^2/R)} = (1 - e^2)^{1/6} \frac{\arcsin(e)}{e}, \quad (\text{A5})$$

$$\tilde{R} \equiv \frac{R}{R_0} = \left(\frac{2}{3A_3(e)(1 - e^2)^{2/3}} \right)^{1/2} \quad (\text{A6})$$

and

$$\tilde{L}^2 \equiv \frac{L^2}{GM^3 R} = \frac{3}{25} (1 - e^2)^{-2/3} \tilde{\Omega}^2 \quad (\text{A7})$$

with $\tilde{\Omega}$ in (65). On the other hand, we expressed also the λ -spin parameter of haloes (1) as a function of the eccentricity only in *Section 3.1.2*, equ.(84). Thus, fixing λ determines the geometric and energetic quantities of the spheroidal halo unambiguously and independently of the BEC particle parameters. Table A1 summarizes them for a range of λ -values which encompass those relevant for CDM haloes. Also, Fig.A1 shows two examples of halo shapes for different spin-parameters.

A3 Compressible, irrotational Riemann-S ellipsoids

The Riemann-S ellipsoid rotates rigidly with angular velocity $\Omega = (0, 0, \Omega)$ like the Maclaurin spheroid. However, on this background rigid rotation, an internal velocity field is superposed specified by two requirements: (i) it shall have a uniform vorticity parallel to Ω ; (ii) it shall leave the ellipsoidal figure unchanged, that is, the velocity vector at any point in the fluid shall be tangent to the isodensity surface passing through that point. The fluid circulation along the equator is given by

$$\oint_C \mathbf{v} \cdot d\mathbf{l} = \pi(2 + f_R) a_1 a_2 \Omega \quad (\text{A8})$$

with $f_R \equiv \zeta'/\Omega$. The flow is irrotational in the rest frame only for $f_R = -2$.

LRS93 have extended the analysis of Chandrasekhar (1969) from incompressible bodies to compressible ones by exploiting the so-called *ellipsoidal approximation* which assumes the following: i) the surfaces of constant density are self-similar ellipsoids (i.e. the axis ratios a_2/a_1 and a_3/a_1 are the same for all interior isodensity surfaces), ii) the density profile $\rho^E(m)$, with m denoting here the mass interior to an isodensity surface, is assumed to be identical to that of a spherical polytrope of same K_p and n , but with radius $R = (a_1 a_2 a_3)^{1/3}$. Both assumptions are strictly valid only in the incompressible limit ($n = 0$), but in the general case, where $n \neq 0$, it provides an approximation to the true equilibrium solution.

Specifying the spin-parameter λ , we can determine the axis ratios (or eccentricities, respectively) using (106) and equation (5.16) in LRS93, which is

$$\frac{4(a_2/a_1)^2}{(1 + (a_2/a_1)^2)^2} - \frac{4B_{12}(a_2/a_1)^2}{\left[(a_3/a_1)^2 A_3 - (a_2/a_1)^2 \frac{A_1 - A_2}{(a_2/a_1)^2 - 1} \right]} \frac{1}{1 + (a_2/a_1)^2} + 1 = 0. \quad (\text{A9})$$

The constants κ_n and q_n in the energy terms appearing in *Section 3.2*, depend on the polytropic index n via

$$\kappa_n \equiv \frac{5}{3} \frac{\int_0^{\chi_1} \theta^n \chi^4 d\chi}{\chi_1^4 |\theta'_1|} \begin{cases} = 1 & \text{for } n = 0 \\ = \frac{5}{3} \left(1 - \frac{6}{\pi^2}\right) \approx 0.653 & \text{for } n = 1 \end{cases} \quad (\text{A10})$$

and

$$q_n \equiv \kappa_n \left(1 - \frac{n}{5}\right) \begin{cases} = 1 & \text{for } n = 0 \\ = \frac{4}{3} \left(1 - \frac{6}{\pi^2}\right) \approx 0.523 & \text{for } n = 1. \end{cases} \quad (\text{A11})$$

$\theta = \rho^S/\rho_c^S$ and $\chi = r/R_{char}$, with $R_{char} = \sqrt{K_p/(2\pi G)}$, are the dimensionless Lane-Emden variables for the density and radius, respectively, of a polytrope. We denote the first zero of the density profile as χ_1 (i.e. $\chi_1 = R_0/R_{char}$) and $\theta_1 = \theta(\chi_1)$.

Now, specializing to $n = 1$, the dimensionless versions of W, R, L in (95), (101), (97) can again be given as functions of the eccentricities only:

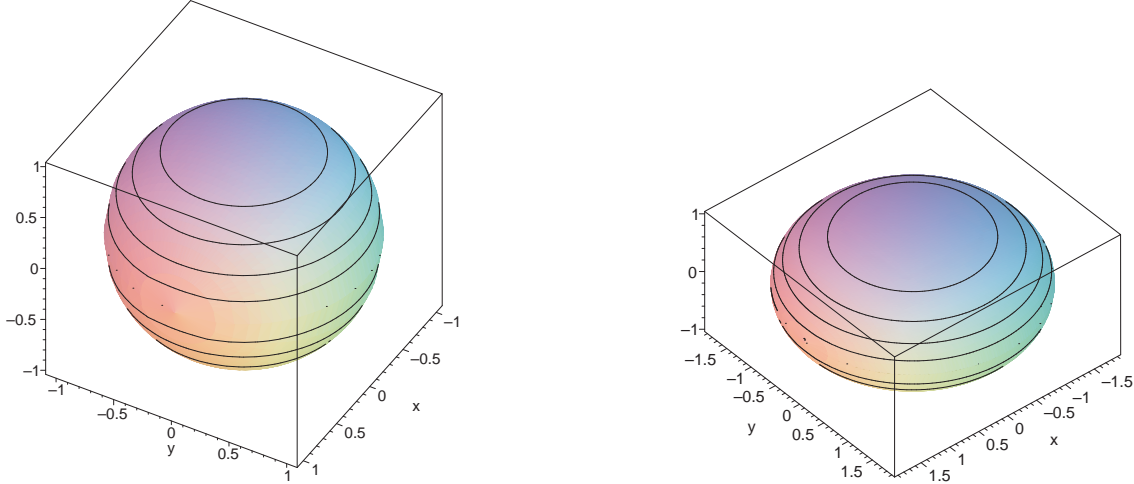
$$|\tilde{W}| \equiv \frac{4}{3} \frac{|W|}{(GM^2/R)} = f(e_1, e_2) \quad (\text{A12})$$

with $f(e_1, e_2)$ in (96),

$$\tilde{R} \equiv \frac{R}{R_0} = [f(e_1, e_2)(1 - 2t)]^{-1/2} \quad (\text{A13})$$

Table A1. Parameters of the homogeneous Maclaurin spheroid as a function of λ

λ	e	t	$\bar{\Omega}$	\bar{L}^2	$ \bar{W} $	\bar{R}
0.01	.6240952030(-1)	.5204(-3)	.4558481107(-1)	.2500065974(-3)	.9999996616	1.000520746
0.02	.1242809380	.207472(-2)	.9086159255(-1)	.1001034014(-2)	.9999946162	1.002083877
0.03	.1850994726	.464440(-2)	.1355078928	.2255299174(-2)	.9999730069	1.004690543
0.04	.2443945077	.819899(-2)	.1792395408	.4016798968(-2)	.9999158013	1.008343664
0.05	.3017559569	.1269872(-1)	.2217968643	.6291209890(-2)	.9997977879	1.013048263
0.06	.3568449744	.1809622(-1)	.2629514670	.9085911668(-2)	.9995887660	1.018812234
0.07	.4093987579	.24338998(-1)	.3025107370	.1241015884(-1)	.9992548016	1.025647448
0.08	.4592299927	.31371503(-1)	.3403173945	.1627516169(-1)	.9987594192	1.033570749
0.09	.5062220297	.39137176(-1)	.3762479967	.2069422508(-1)	.9980646348	1.042605066
0.10	.5503211259	.47580078(-1)	.4102099657	.2568290981(-1)	.9971317748	1.052780577
0.20	.8470361891	.1590675677	.6351541756	.1124337842	.9662629271	1.231978660
0.30	.9658444276	.3004590826	.6495893878	.3065151508	.8638313134	1.703156470


Figure A1. Maclaurin spheroidal halo rotating about the z -axis having $a_3 = 1$ and $\lambda = 0.05$ (left-hand-plot) and $\lambda = 0.2$ (right-hand-plot), respectively.

(see (101)), and

$$\tilde{L}^2 \equiv \frac{L^2}{GM^3R} = \frac{3}{4} \left(\frac{\kappa_1}{5} \right)^2 \gamma^2(e_1, e_2) \bar{\Omega}^2 \quad (\text{A14})$$

where

$$\gamma(e_1, e_2) \equiv \left[(1 - e_1^2)^{-1/3} (1 - e_2^2)^{-1/3} + (1 - e_1^2)^{2/3} (1 - e_2^2)^{-1/3} - 4 \frac{(1 - e_1^2)^{1/3} (1 - e_2^2)^{-2/3}}{(1 - e_1^2)^{-1/3} (1 - e_2^2)^{-1/3} + (1 - e_1^2)^{2/3} (1 - e_2^2)^{-1/3}} \right] \quad (\text{A15})$$

and $\bar{\Omega}$ in (94). The angular velocity of the internal motions Λ is related to $\bar{\Omega}$ via (93), defining $\tilde{\Lambda} \equiv \Lambda/\Omega_G$. The λ -spin parameter determines the above quantities unambiguously via equ.(106). Table A2 summarizes them for a range of λ -values, encompassing those relevant for CDM haloes. Note that $\tilde{\Lambda}$ is a monotonically decreasing function of λ , while $\bar{\Omega}$ is *not* monotonic, in contrast to the case of the Maclaurin spheroid. Two illustrative examples of halo shapes can be found in Fig.A2.

A3.1 Density profile for $n = 1$

LRS93 confirm their results by numerical comparison of the density profiles of rotating versus non-rotating configurations for different polytropic indices n . However, we observe that the ellipsoidal approximation in conjunction with the

known analytic density profile of the equilibrium ($n = 1$)-sphere, equ.(35), makes possible the derivation of an analytic profile for a rotating, ellipsoidal ($n = 1$)-polytrope, as follows.

According to the ellipsoidal approximation, $\rho^S(m)/\bar{\rho}^S$ and $\rho^E(m)/\bar{\rho}^E$ have the same dependence on m/M . From this follows that the shapes of the cumulative mass profiles are the same. The ellipsoid has a larger volume, however, than the equilibrium sphere according to (101). Since we consider the case where the total mass M shall be the same, this means that the mean densities (and hence central densities) are different according to (139).

Now, the equation of an ellipsoidal isodensity surface can be written as

$$q^2 = x^2 + \frac{y^2}{1 - e_1^2} + \frac{z^2}{1 - e_2^2}, \quad (\text{A16})$$

whose dimensionless form, after dividing by R_{char} , will be denoted carrying a 'tilde'-sign as

$$\tilde{q} \equiv q/R_{char}. \quad (\text{A17})$$

The outer surface of the ellipsoid is then given by

$$\tilde{q}_{max}^2 = \tilde{x}^2 + \frac{\tilde{y}^2}{1 - e_1^2} + \frac{\tilde{z}^2}{1 - e_2^2} = \frac{a_1^2}{R_{char}^2}. \quad (\text{A18})$$

Writing the semi-major axis in terms of mean radius and eccentricities equ.(87), and using (101), we see that

$$\tilde{q}_{max} = \frac{\pi g(e_1, e_2)^{-1/2}}{(1 - e_1^2)^{1/6} (1 - e_2^2)^{1/6}}. \quad (\text{A19})$$

Since the isodensity surfaces are self-similar ellipsoids, it follows more generally that

$$\tilde{q} = \frac{\chi g(e_1, e_2)^{-1/2}}{(1 - e_1^2)^{1/6} (1 - e_2^2)^{1/6}}, \quad (\text{A20})$$

with χ from above. Because of (101), the volumes differ according to $V^E = V^S g(e_1, e_2)^{-3/2}$ and correspondingly we have for the volume elements that

$$dV^E = dV^S g(e_1, e_2)^{-3/2} \\ = 4\pi R_{char}^3 (1 - e_1^2)^{1/2} (1 - e_2^2)^{1/2} \tilde{q}^2 d\tilde{q}. \quad (\text{A21})$$

Using now the fact that the shapes of the cumulative mass profiles are the same, we can derive the following density profile of the $(n = 1)$ -polytropic ellipsoids,

$$\rho^E(\tilde{q}) = \rho_c^E \frac{\sin \left[\tilde{q} (1 - e_1^2)^{1/6} (1 - e_2^2)^{1/6} g(e_1, e_2)^{1/2} \right]}{\tilde{q} (1 - e_1^2)^{1/6} (1 - e_2^2)^{1/6} g(e_1, e_2)^{1/2}} \quad (\text{A22})$$

with \tilde{q} from above and with ρ_c^E , as usual, denoting the central density of the ellipsoid. Using this density profile, the total mass can be calculated to be

$$M^E = 4\pi^2 R_{char}^3 \rho_c^E g(e_1, e_2)^{-3/2} = 4\pi^2 R_{char}^3 \rho_c^S = M^S, \quad (\text{A23})$$

i.e. the mass of the $(n = 1)$ -polytropic ellipsoid is the same as that for the equilibrium $(n = 1)$ -sphere, as we have demanded.

APPENDIX B: SPLITTING OF THE GROSS-PITAEVSKII ENERGY FUNCTIONAL

In this appendix, equ. (114) to (116) are derived. All energies and wave functions, ψ, f, w , as well as the respective amplitudes and phases, S, S_0, S_w , are those in the rotating frame of reference, so primes are omitted in this section altogether. The integrations are over the whole space.

We insert (110) into the energy functional (107) considering each term separately: the kinetic energy term has the following form,

$$\int \frac{\hbar^2}{2m} |\nabla \psi|^2 = \int \frac{\hbar^2}{2m} \left\{ f^2 |\nabla w|^2 + |w|^2 [f^2 (\nabla S_0)^2 + (\nabla f)^2] \right. \\ \left. + \frac{1}{2} \nabla(f^2) \cdot \nabla(|w|^2) + f^2 \nabla S_0 \cdot (i w \nabla w^* - i w^* \nabla w) \right\}. \quad (\text{B1})$$

The rotation term is given by

$$-i\hbar \int \psi^* \mathbf{\Omega} \cdot (\nabla \psi \times \mathbf{r}) = \\ = i\hbar \int f^2 w^* \nabla w \cdot (\mathbf{\Omega} \times \mathbf{r}) - \hbar \int f^2 |w|^2 \nabla S_0 \cdot (\mathbf{\Omega} \times \mathbf{r}), \quad (\text{B2})$$

while the potential energies due to gravitation and self-interaction are simply

$$\int \left(\frac{m}{2} \Phi |\psi|^2 + \frac{g}{2} |\psi|^4 \right) = \int \left(\frac{m}{2} \Phi f^2 |w|^2 + \frac{g}{2} f^4 |w|^4 \right). \quad (\text{B3})$$

It is advantageous to write the energy such that the vortex-free contribution is clearly separated from the other terms. Using the above expressions, we may thus recast the functional into the following form

$$\mathcal{E}[\psi] = \mathcal{E}[f e^{iS_0}] + \int \frac{\hbar^2}{2m} (|w|^2 - 1) \times$$

$$\times \left[(\nabla f)^2 + f^2 (\nabla S_0)^2 - \frac{2m}{\hbar} f^2 \nabla S_0 \cdot (\mathbf{\Omega} \times \mathbf{r}) \right] + \\ + \int \frac{m}{2} f^2 [\Phi |w|^2 - \Phi_0] + \int \frac{\hbar^2}{4m} \nabla(f^2) \cdot \nabla(|w|^2) \\ + \int \frac{\hbar^2}{2m} f^2 |\nabla w|^2 + \frac{g}{2} \int f^4 (|w|^4 - 1) + \\ + \int \frac{\hbar^2}{2m} [f^2 \nabla S_0 \cdot (i w \nabla w^* - i w^* \nabla w) + \\ i \frac{2m}{\hbar} f^2 w^* \nabla w \cdot (\mathbf{\Omega} \times \mathbf{r})] \quad (\text{B4})$$

with $\mathcal{E}[f e^{iS_0}]$ being the vortex-free energy of equ.(113). Evaluating the second term in line 3 results in

$$\int \nabla(f^2) \cdot \nabla(|w|^2) = \int \nabla(f^2) \cdot \nabla(|w|^2 - 1) = \\ - \int (|w|^2 - 1) \Delta(f^2) = -2 \int (|w|^2 - 1) (f \Delta f + (\nabla f)^2), \quad (\text{B5})$$

which, by using (111), becomes

$$\int \frac{\hbar^2}{4m} \nabla(f^2) \cdot \nabla(|w|^2) = \int \frac{\hbar^2}{2m} (|w|^2 - 1) \times \\ \times \left[\frac{2m}{\hbar} f^2 \nabla S_0 \cdot (\mathbf{\Omega} \times \mathbf{r}) - f^2 (\nabla S_0)^2 - \right. \\ \left. - \frac{2m}{\hbar^2} f^2 (m \Phi_0 + g f^2 - \nu) - (\nabla f)^2 \right], \quad (\text{B6})$$

assuming that the halo mass density either goes to zero as $|\mathbf{r}| \rightarrow \infty$ or is identically zero beyond some finite radius. Furthermore, we take advantage of rewriting the following terms:

$$\frac{g}{2} \int f^4 (|w|^4 - 1) \equiv g \int f^4 (|w|^2 - 1) + \frac{g}{2} \int f^4 (1 - |w|^2)^2 \quad (\text{B7})$$

and

$$\int \left[\frac{\hbar^2}{2m} f^2 \nabla S_0 \cdot (i w \nabla w^* - i w^* \nabla w) + i \hbar f^2 w^* \nabla w \cdot (\mathbf{\Omega} \times \mathbf{r}) \right] = \\ = - \frac{\hbar^2}{m} \int i f^2 w^* \nabla w \cdot \left(\nabla S_0 - \frac{m}{\hbar} \mathbf{\Omega} \times \mathbf{r} \right), \quad (\text{B8})$$

respectively, using the conservation of particle number, $\int (|w|^2 - 1) f^2 \mu = 0$. Collecting all of the above expressions, we shall finally arrive at the following splitting of the energy functional:

$$\mathcal{E}[\psi] = \mathcal{E}[f e^{iS_0}] + \mathcal{G}_f[w] - \mathcal{R}_f[w], \quad (\text{B9})$$

where

$$\mathcal{G}_f[w] \equiv \int \left(\frac{\hbar^2}{2m} f^2 |\nabla w|^2 + \frac{g}{2} f^4 (1 - |w|^2)^2 \right) + \\ + \int \left(\frac{m}{2} f^2 \Phi_0 + \frac{m}{2} f^2 |w|^2 [\Phi - 2\Phi_0] \right) \quad (\text{B10})$$

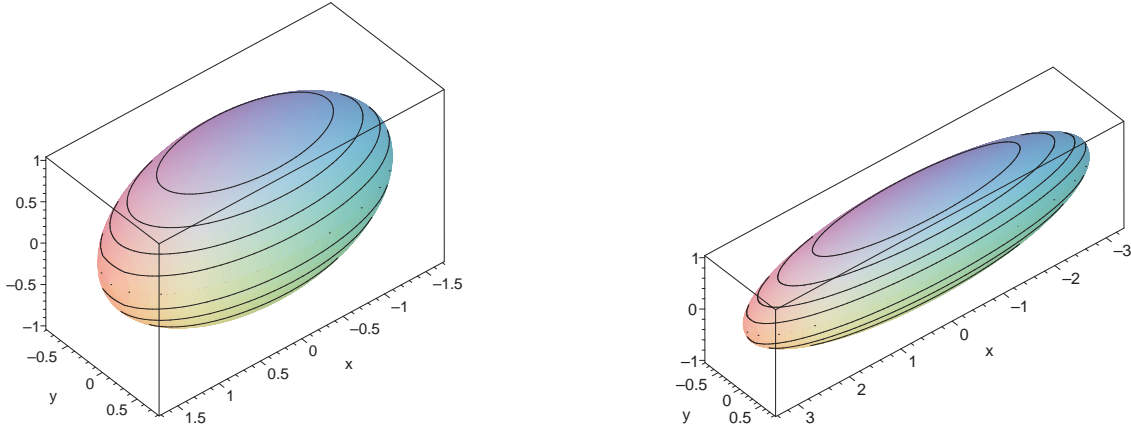
and

$$\mathcal{R}_f[w] \equiv \int i f^2 w^* \nabla w \cdot \left(\nabla S_0 - \frac{m}{\hbar} \mathbf{\Omega} \times \mathbf{r} \right). \quad (\text{B11})$$

Table A2. Parameters of the irrotational, ($n = 1$)-polytropic Riemann-S ellipsoid as a function of λ

λ	a_2/a_1	a_3/a_1	e_1	e_2	t
0.01	.7073606352	.8191876671	.7068528360	.5735255584	.8990308186(−3)
0.02	.6157806530	.7444171156	.7879176273	.6677148778	.3256446859(−2)
0.03	.5551042656	.6884452492	.8317807730	.7252883143	.6676951963(−2)
0.04	.5095561821	.6425906919	.8604373872	.7662096337	.1087731987(−1)
0.05	.4731628114	.6033952054	.8809750019	.7974423027	.1565115011(−1)
0.06	.4429370293	.5690393124	.8965527247	.8223103191	.2084571079(−1)
0.07	.4171522426	.5384160866	.9088366226	.8426791309	.2634641496(−1)
0.08	.3947154535	.5107881879	.9188034125	.8597065936	.3206621692(−1)
0.09	.3748897504	.4856329988	.9270694014	.8741627940	.3793824738(−1)
0.10	.3571546372	.4625629986	.9340452693	.8865864156	.4391062656(−1)
0.20	.2417900586	.3025300680	.9703285874	.9531398418	.1032663262
0.30	.1766421365	.2101855698	.9842751422	.9776615090	.1550787050

λ	$\bar{\Omega}$	$\bar{\Lambda}$	\bar{L}^2	$ \bar{W} $	\bar{R}
0.01	.7169963591	.6760714962	.8424269299(−6)	.9919850657	1.004935593
0.02	.7176346622	.6408208912	.3253671535(−5)	.9842263532	1.011279929
0.03	.7165548594	.6081343468	.7088561436(−5)	.9766699520	1.018697841
0.04	.7140826379	.5777254698	.1223320264(−4)	.9692743288	1.026958151
0.05	.7104728779	.5493488048	.1859786170(−4)	.9620070989	1.035897363
0.06	.7059271906	.5227939592	.2611162661(−4)	.9548427521	1.045397324
0.07	.7006067868	.4978802570	.3471838378(−4)	.9477609961	1.055371038
0.08	.6946418722	.4744520038	.4437376265(−4)	.9407455674	1.065753362
0.09	.6881386566	.4523744952	.5504279856(−4)	.9337833787	1.076494765
0.10	.6811846403	.4315306946	.6669814241(−4)	.9268637895	1.087557099
0.20	.5984642204	.2734205668	.2348312504(−3)	.8587224921	1.211459922
0.30	.5100096167	.1747264833	.49746267360(−3)	.7911442386	1.353621249


Figure A2. Irrotational Riemann-S ellipsoidal halo rotating about the z -axis having $a_3 = 1$ and $\lambda = 0.05$ (left-hand-plot) and $\lambda = 0.2$ (right-hand-plot), respectively.

APPENDIX C: THE CHEMICAL POTENTIAL OF BEC HALOES

We have dealt in this paper mostly with the energy of a given BEC halo. The equation of motion for stationary systems in equ.(51) also involve the chemical potential μ , which is fixed by the conservation of particles. For a static ground state without vortex, (51) easily leads to the following expression for the equilibrium condensate chemical potential

$$\mu = -\frac{\hbar^2}{2m} \frac{\Delta\sqrt{n}}{\sqrt{n}} + m\Phi + gn \quad (\text{C1})$$

with corresponding time-independent particle number density $n = |\psi|^2$. Multiplying (54) with $\partial\psi^*/\partial N$ results in the well-known thermodynamic relationship, $\mu = \partial E/\partial N$, where E is the total energy of the BEC halo wave function under consideration. In the TF regime, for instance, (C1) reduces to $\mu = g\rho/m + m\Phi$. Multiplying by ρ and integrating results in $\mu = 2mE/M$, where E is the energy in the Thomas-Fermi regime, i.e. (55) with $K_Q = 0$ (and $T = 0$ if $\mathbf{v} = 0$). The chemical potential for ($n = 1$)-polytropic BEC haloes is thus given by

$$\mu = 2\frac{E}{N}. \quad (\text{C2})$$

We can derive this relationship also by using the energy expressions of LRS93. The total energy of the polytropic sphere with index n according to LRS93 is

$$E = U + W = k_1 K(\rho_c^S)^{1/n} M - k_2 (\rho_c^S)^{1/3} G M^{5/3}, \quad (\text{C3})$$

where the constants k_1, k_2 depend on n , χ_1 and θ'_1 . Using the formula for the central density of the sphere (see also (36))

$$\rho_c^S = \frac{1}{3} \frac{\chi_1}{|\theta'_1|} \bar{\rho}^S = \frac{\chi_1}{4\pi|\theta'_1|} \frac{M}{R^3} \equiv g_1 \frac{M}{R^3}, \quad (\text{C4})$$

we rewrite

$$E = k_1 K g_1^{1/n} \frac{(Nm)^{1/n+1}}{R^{3/n}} - k_2 g_1^{1/3} \frac{G}{R} (Nm)^2. \quad (\text{C5})$$

The chemical potential of this sphere is thus

$$\mu = \frac{\partial E}{\partial N} = \left(\frac{1}{n} + 1\right) \frac{U}{N} + 2\frac{W}{N} = \frac{1}{N} \left(E + \frac{U}{n} + W\right), \quad (\text{C6})$$

which reduces to $\mu = 2E/N$ for $n = 1$, in accordance with (C2).